Osaka University, and the National Institute of Neuroscience, National Center of Neurology and Psychiatry.

Pharmacological Agents—Haloperidol, the dopamine D_2-R-selective antagonist L-741,626 (21), and the D_2-R-selective agonist (−)-quinpirole were purchased from Sigma. The drugs were administered by intraperitoneal injection in a volume of 10 μl/g body weight. All solutions were prepared immediately prior to the experiments. To exclude the effect of drug tolerance, no animals were used more than once in the pharmacological experiments.

Antibodies—Goat polyclonal anti-D_2-R antibody (N19) was purchased from Santa Cruz Biotechnology (Santa Cruz, CA). Rabbit polyclonal anti-tyrosine hydroxylase (TH) antibody was obtained from Chemicon (Temecula, CA). A mouse monoclonal anti-phosphotyrosine antibody (Tyr(P)-100) was purchased from Cell Signaling Technology (Beverly, MA). Phosphorylation site-specific rabbit polyclonal antibody against p-Src (Y418) and p-Src (Y529) was obtained from BIOSOURCE (Camarillo, CA) and against p-NR2B (Y1472) was from Sigma. Rabbit polyclonal anti-NR2B antibody was a gift from Dr. Masahiko Watanabe (22). Anti-Src mouse monoclonal antibody (GD11) was purchased from Upstate Biotechnology, Inc. (Lake Placid, NY). The anti-Fyn rat monoclonal antibody (γC3) was raised by Dr. Masahiro Yasuda (23). The anti-βIII tubulin mouse monoclonal antibody was purchased from Promega (Madison, WI).

Assessment of Catalepsy—Catalepsy was measured by a bar test (24). The test was carried out 1 h after intraperitoneal injection of haloperidol (0–1.0 mg/kg) or L-741,626 (0–10 mg/kg). A 3-mm-diameter wooden bar was fixed horizontally 4 cm above the floor of a Plexiglas cage. The animals were placed inside the test cage and allowed to acclimatize for 5 min prior to performing the bar test. Both forepaws were then gently placed on the bar, and the length of time during which each mouse maintained the initial position was measured (maximum cut-off time, 180 s).

Analysis of Rigidity—Muscle rigidity after haloperidol administration was assessed by a mechanographic technique using a modified device designed for rat experiments (25). The mouse was placed in a narrow, well ventilated plastic tube to restrict body movement, and one hind leg was bound to a force sensor (AD4937-5N, A & D Co. Ltd., Tokyo, Japan) that records linear reciprocating motion (15-mm distance, 15 cycles/min) via a crank and motor. The raw data from the force sensor were analyzed on a Macintosh computer connected to an A/D converter and software (PowerLab 4s, chart version 3.6 ADInstruments, Mountain View, CA), and the resistance of the flexor and extensor muscles to forced extension and flexion of the knee and ankle joint was measured. The mice were attached to the above device, and the difference in muscle resistance before and after the administration of vehicle or haloperidol (1.0 mg/kg) was recorded. The mean amplitude of 10 consecutive waves at each time point was calculated. Spikes that indicated spontaneous movements of the mice were excluded from the count.

In Situ Hybridization Histochemistry—The distribution of D_2-R gene expression in the striatum of the control and Fyn-deficient mice was compared. The probe was prepared as follows. A cDNA fragment encoding the sequence of mouse D_2-R (1.3 kbp, a gift from Dr. T. Kaneko, Kyoto University) was cloned into the pBluescript II/KS− vector, and the clone was digested and used as a DNA template to synthesize an antisense or sense digoxigenin-labeled cRNA probe. The probe was prepared with T7 or T3 RNA polymerase and a digoxigenin RNA labeling kit (Roche Applied Science). Staining was performed as reported previously (26). The sense cRNA probe was employed as the control, and no signals in the brain were detected with it.

Immunoblot Analysis—One hour after administration of the vehicle, haloperidol (1.0 mg/kg), or L-741,626 (5 mg/kg), the striatum was immediately dissected and frozen in liquid nitrogen. The striatum was placed in buffer containing 10% sucrose, 3% SDS, 10 mM Tris-HCl, pH 6.8, 1 mM sodium orthovanadate, and 1 mM phenylmethylsulfonyl fluoride and homogenized with a Polytron homogenizer (Kinematica AG, Lucerne, Switzerland). Samples were spun down (20,000 × *g*, 15 min) to remove insoluble material, and the protein concentration was determined with the BCA protein assay reagent (Pierce). After the addition of 40 mM dithiothreitol, the samples were boiled for 5 min, and an equal amount of protein (40 μg per lane) from each sample was separated by electrophoresis on 10% polyacrylamide gels. The gels were transferred onto Immobilon membranes (Millipore, Bedford, MA). The membranes were blocked with 1% bovine serum albumin in Tris-buffered saline (TBS; pH 7.5) containing 0.1% Tween 20 (TBS-T) or 10% skim milk in TBS-T for 1 h and probed with primary antibodies (1:750 dilution for TH, 1:4000 for anti-βIII tubulin, and 1:1000 for other antibodies). After washing three times with TBS-T, the membranes were incubated with horseradish peroxidase-labeled secondary antibodies (anti-goat, anti-rabbit, anti-rat, or anti-mouse IgG, 1:20,000 dilution, all purchased from The Jackson Laboratories, West Grove, PA). After washing three times, the signals were detected with ECL Plus (Amersham Biosciences) and ATTO Cool Saver (ATTO Corp., Tokyo, Japan). The membranes were then incubated with stripping buffer (100 mM 2-mercaptoethanol, 2% SDS, 62.5 mM Tris-HCl, pH 6.7) at 50 °C for 30 min, washed, blocked, and reprobed with other antibodies.

Immunoprecipitation and Western Blotting—The procedures for immunoprecipitation were as described previously (15). Striatum obtained 1 h after vehicle or haloperidol (1.0 mg/kg) administration was placed in lysis buffer (10 mM Tris-HCl, pH 7.4, 1% Triton X-100, 0.1% sodium deoxycholate, 0.1% SDS, 0.15 M NaCl, 1 mM EDTA, and 1 mM sodium orthovanadate) and homogenized with a Polytron homogenizer. Samples were spun down to remove insoluble material, and the protein concentration was determined. Equal amounts of protein (500 μg) were then used for immunoprecipitation. Samples were precleared with protein G-Sepharose (Amersham Biosciences), incubated for 1 h at 4 °C with 1 μg of the anti-Fyn or anti-Src antibody, and then incubated for 1 h at 4 °C with 10 μl of protein G-Sepharose. After three washes with lysis buffer, the pelleted protein G-Sepharose was boiled for 5 min in 30 μl of SDS sample buffer, and 15 μl of the supernatant was subjected to SDS-PAGE. The separated proteins were subsequently blotted onto Immobilon, probed with each antibody, and visualized as described above.

Primary Cultures of Striatal Neurons—Primary cultures of striatal neurons were prepared from the fetal striata of wild-type and Fyn-deficient mice at embryonic day 17. Striata from 6 to 8 fetal brains were dissected and placed in Hanks' balanced salt solution (Invitrogen) and then were transferred into a dissociation medium containing Hanks' balanced salt solution, 0.05% DNase I, and 1% trypsin/EDTA and incubated at 37 °C for 7 min. After sedimentation, the supernatant was removed, and the pellet was washed three times with Hanks' balanced salt solution containing 1% penicillin/streptomycin. The tissue was gently placed in Hanks' balanced salt solution containing 0.05% DNase I and triturated with a plastic pipette until a homogeneous suspension was obtained. After centrifugation at 130 × *g* for 8 min, the cell pellet was resuspended in Neurobasal/B27 medium (Invitrogen) containing 0.5 mM L-glutamine and penicillin/streptomycin (100 units/ml). The cell cultures were seeded at a density of 3×10^5 cells/cm^2 on 0.1% polyethyleneimine-coated cover glasses in 1.9 cm^2/well dishes (Nunclon, Nunc). Cells were maintained at 37 °C under a humidified 5% CO_2

atmosphere. The cultured striatal neurons were identified immunocytochemically with anti-GAD65 antibody (Chemicon) and anti-MAP2 antibody (Sigma). More than 95% of both the wild-type and Fyn-deficient neurons were double-labeled by anti-GAD65 and anti-MAP2 (supplemental Fig. S1).

Calcium Imaging—Calcium imaging was carried out as described previously (27). Briefly, striatal primary cells were incubated with 10 μM fura-2/AM (Dojindo) for 1 h at 30 °C in balanced salt solution (BSS) consisting of (in mM) NaCl 130, KCl 5.4, glucose 5.5, HEPES 10, and $CaCl_2$ 2, and adjusted to pH 7.4 with NaOH. After washing, the cover glasses that contained cultured neurons were mounted on the stage of an inverted fluorescence microscope (IX50; Olympus) and perfused with BSS at a flow rate of 1.8 ml/min. The perfusion medium was pre-warmed and maintained at 32.6 ± 1.1 °C in the measurement dish. Fluorescence images obtained by alternate excitation with 340 and 380 nm light through the ×20 objective lens and CCD camera (C2400-8; Hamamatsu Photonics, Hamamatsu, Japan) were fed into an image processor (Argus 50, Hamamatsu) for ratiometric analysis. The effect of the D_2-R antagonist L-741,626 on the channel activity of NMDA receptors was investigated in the presence of the selective D_2-R agonist quinpirole in the perfusion medium. As shown in supplemental Fig. S2, quinpirole alone had a dose-dependent inhibitory effect on the channel activity of the NMDA receptors of the striatal primary neurons of the control mice consistent with its inhibitory effect reported in the striatal slice culture (28). Quinpirole was observed to have almost the same degree of the inhibitory effect on Fyn-deficient neurons (49% decrease at 50 μM).

Preparation of Protein Samples from the Cultured Neurons—Striatal neurons were cultured in 1.9 cm^2/well dishes (Nunclon, Nunc) as described above. Each solution used in the following experiments was pre-warmed to 37 °C in a water bath. Culture dishes were warmed on a heat block to 37 °C. The culture medium was removed, and the cultured cells were incubated with BSS for at least 5 min. The cells were then incubated with the following: 1) BSS for 7 min followed by incubation in quinpirole (50 μM) in BSS for 7 min, or 2) in quinpirole (50 μM) in BSS for 7 min followed by a mixture of quinpirole (50 μM) and L-741,626 (10 μM) in BSS for 7 min. The solution was removed, and the cells were immediately lysed in 150 μl of SDS sample buffer.

Statistical Analyses—The results of the catalepsy assessment and calcium imaging were evaluated by the Kruskal-Wallis test followed by the Mann-Whitney *U* test. The results of the muscle rigidity analysis were evaluated by a two-way repeated measure ANOVA. The results of Western blotting were evaluated by one-way ANOVA followed by Bartlett's test. All data are expressed as the mean ± S.E.

RESULTS

Haloperidol induced catalepsy in the $+/fyn^Z$ mice, and the duration of the catalepsy increased in a dose-dependent manner (Fig. 1). By contrast, the duration of the catalepsy in the fyn^Z/fyn^Z mice was significantly shorter (Fig. 1). At the 1.0 mg/kg dose, there was no difference in the cataleptic response between the $+/fynZ$ mice and the wild-type mice (154.5 ± 47.1 s). The D_2-R-selective antagonist L-741,626 was confirmed to induce catalepsy in the control mice (supplemental Fig. S3), as reported previously in rats (29), but the duration of the catalepsy was significantly reduced in fyn^Z/fyn^Z mice (supplemental Fig. S3). Because there was no significant difference in the temporal patterns of the locomotor activity between $+/fyn^Z$ mice and fyn^Z/fyn^Z mice (30), the altered cataleptic response in the fyn^Z/fyn^Z mice was concluded not to be due to a locomotion defect.

Because Fyn-deficient mice are more fearful than control mice (31),

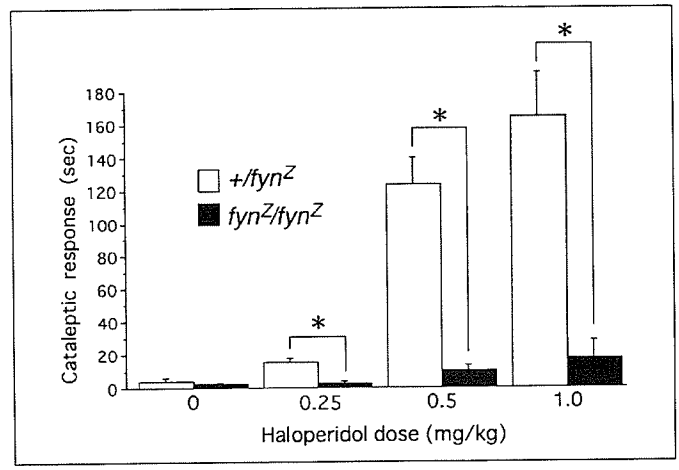

FIGURE 1. **Assessment of catalepsy following haloperidol administration.** The cataleptic response to haloperidol administration increased dose-dependently in $+/fyn^Z$ mice but was significantly reduced in fyn^Z/fyn^Z mice. Eight to twelve animals were used in each group. The *columns* represent the means, and the *bars* represent the S.E. Statistically significant differences were identified by the Mann-Whitney *U* test; *, $p < 0.001$.

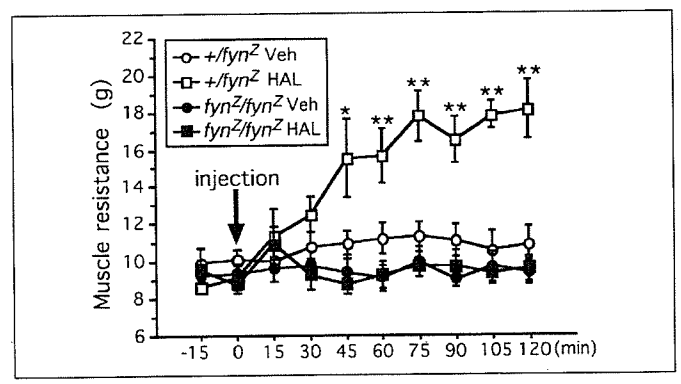

FIGURE 2. **Mean amplitude of muscle resistance before and after haloperidol (*HAL*) injection.** In $+/fyn^Z$ mice, muscular rigidity increased as early as 45 min after haloperidol administration (1 mg/kg), and the increase persisted for more than 2 h. By contrast, no increase in muscle rigidity was detected in the fyn^Z/fyn^Z mice after haloperidol administration. Administration of vehicle (*Veh*) alone did not affect rigidity in either genotype. Six animals were used in each group. Data are expressed as means ± S.E. Statistically significant differences were identified by two-way repeated measure ANOVA; *, $p < 0.05$; **, $p < 0.005$.

we suspected that they might avoid a procedure like the "bar test" and that the duration of catalepsy would be misleadingly short as a result. We therefore also measured muscular rigidity to minimize any such emotional influence on the response to haloperidol. Haloperidol induced a marked increase in hind limb muscle rigidity in the $+/fyn^Z$ mice that was detectable as early as 45 min after administration (1.0 mg/kg) and persisted for more than 2 h, but no increase in muscle rigidity was detected in the fyn^Z/fyn^Z mice (Fig. 2 and supplemental Fig. S4).

To exclude the possibility that the failure to respond to haloperidol was because of a difference in D_2-R expression, *in situ* hybridization of D_2-R mRNA and Western blotting of D_2-R protein were performed on the striatum of $+/fyn^Z$ and fyn^Z/fyn^Z mice. As shown in Fig. 3, no clear difference was observed in either striatal D_2-R gene expression (Fig. 3*A*) or the protein level (Fig. 3*B*). Western blotting analysis of striatal TH was also performed to determine whether there was any difference between the two genotypes in the abundance of the rate-limiting enzyme in dopamine biosynthesis, but little difference in the amount of TH protein was found (Fig. 3*C*).

The effect of haloperidol on protein tyrosine phosphorylation in the

striatum of the $+/fyn^Z$ and fyn^Z/fyn^Z mice was compared by Western blotting. One hour after haloperidol administration (1.0 mg/kg), a marked increase in tyrosine phosphorylation of several proteins, including 60-, 110-, and 180-kDa proteins, was observed in the striatum of the $+/fyn^Z$ mice but not of the fyn^Z/fyn^Z mice (Fig. 4*A*).

Because the 60-kDa protein corresponds in size to SFKs, we measured tyrosine phosphorylation of the activation-related Tyr-418 residue on SFKs. As shown in Fig. 4*B*, phospho-Tyr-418 increased after haloperidol injection of the $+/fyn^Z$ mice, but no such effect was observed in the fyn^Z/fyn^Z mice. Basal Tyr(P)-418 immunoreactivity was much lower in the fyn^Z/fyn^Z mice. Because the anti-pY418 antibody recognizes both Fyn and Src, we immunoprecipitated Fyn and Src, and we examined the phosphorylation of the activation-related residue, Tyr-418, and of the inhibition-related residue, Tyr(P)-529, by Western blotting in the $+/fyn^Z$ mice. As shown in Fig. 4*C*, Fyn but not Src was activated at Tyr-418 by haloperidol, and no change was observed in the phosphorylation at Tyr-529. Because the 180-kDa protein corresponds in size to the NR2B subunit, we also measured the phosphorylation of the Tyr-1472 of NR2B, the key phosphorylation site, by Fyn. The results showed that phospho-Tyr-1472 increased in the $+/fyn^Z$ mice but not in the fyn^Z/fyn^Z mice (Fig. 4*D*). The basal level of Tyr(P)-1472 in the fyn^Z/fyn^Z mice was not significantly different from the basal level in the $+/fyn^Z$ mice. Marked increases in tyrosine phosphorylation of the 60-, 110-, and 180-kDa proteins and up-regulation of Tyr(P)-418 and Tyr(P)-1472 were also observed following L-741,626 administration to the control mice, but no such effects were observed in the fyn^Z/fyn^Z mice (supplemental Fig. S5).

There were no sex differences in the results of either the behavioral or biochemical studies (data not shown). The same findings in regard to the haloperidol-induced enhancement of tyrosine phosphorylation were also observed in the wild-type mice, and no clear difference was detected between $+/fyn^Z$ mice and wild-type mice (data not shown). To investigate whether the Fyn-mediated increase in NMDA receptor phosphorylation by D_2-R blockade affects NMDA receptor activity, we prepared striatal primary cultures and assessed the channel activity of NMDA receptors by the calcium imaging method.

After 4–7 days of culture, we loaded 10 μM fura-2/AM into the primary cells and measured the increase in intracellular calcium concentration ($[Ca^{2+}]_i$) by calcium fluorimetry. Exposure to 3 μM NMDA/10 μM glycine for 30 s induced a robust response in more than 95% of the cells analyzed, and repeated applications of NMDA/glycine at 5-min intervals evoked reproducible responses (data not shown), indicating little desensitization of the NMDA receptors under our experimental conditions.

We first examined the effect of a D_2-R-selective antagonist,

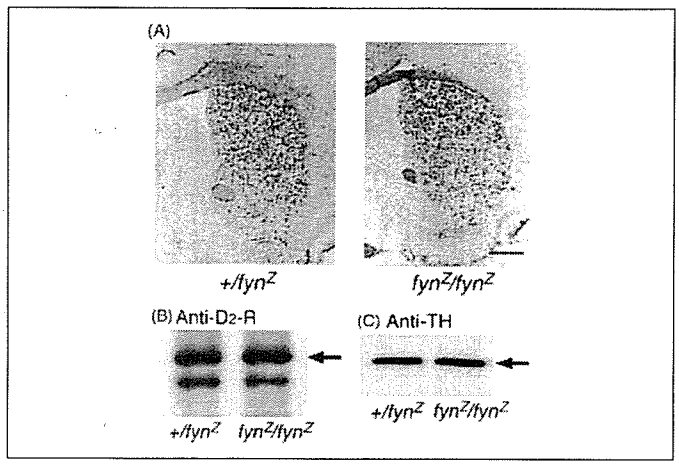

FIGURE 3. **Expression of dopaminergic markers in the striatum.** *A, in situ* hybridization histochemistry for dopamine D_2 receptor mRNA. Strong D_2 receptor expression in the striatum was seen in both genotypes, and there was little difference in its distribution. *Scale bar*, 500 μm. *B*, Western blotting analysis of the dopamine D_2 receptor in the striatum. The intensity of the upper band (*arrow*) around 85 kDa, corresponding to the D_2-receptor, was essentially the same in both genotypes. *C*, Western blotting analysis of striatal tyrosine hydroxylase (*TH*). The intensity of the band at around 70 kDa differed little between the two genotypes.

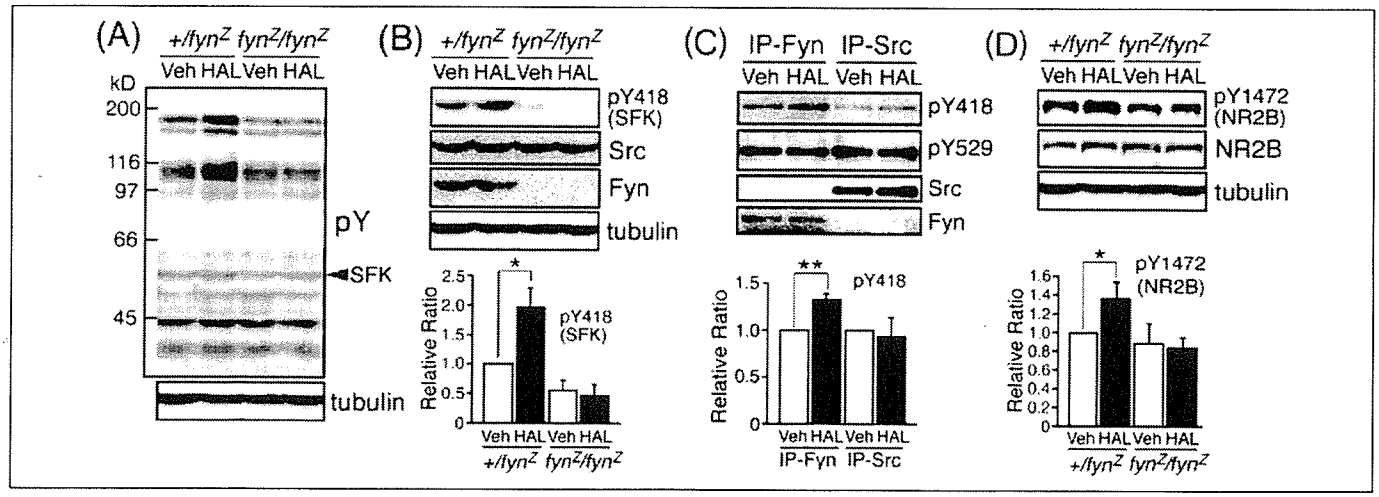

FIGURE 4. **Tyrosine phosphorylation in the striatum after haloperidol administration.** *A*, haloperidol (*HAL*) administration (1.0 mg/kg) increased the tyrosine phosphorylation of several proteins, including 60-, 110-, and 180-kDa proteins, in $+/fyn^Z$ mice compared with vehicle (*Veh*) administration, but no such difference was found in the fyn^Z/fyn^Z mice. *B*, the same tendency toward a haloperidol-induced increase in tyrosine phosphorylation was observed in regard to Tyr-418 of Src family kinases (pY418) in the $+/fyn^Z$ mice, but no such increase was observed in the fyn^Z/fyn^Z mice. The amounts of Src and Fyn were unchanged. Densitometric analysis revealed a significant increase in the band density of the Tyr(P)-418 of Src family kinases after injection in $+/fyn^Z$ mice with haloperidol. No such increase was detected in the fyn^Z/fyn^Z mice, and the basal band density was also much lower in fyn^Z/fyn^Z mice. *C*, haloperidol-induced increase in the phosphorylation of the Src family kinases Src and Fyn in the control mice demonstrated by immunoprecipitation (*IP*) and Western blotting. Haloperidol (1.0 mg/kg) induced an increase in Tyr(P)-418 following anti-Fyn immunoprecipitation but not following anti-Src immunoprecipitation. No clear change was observed in Tyr(P)-529. The amounts of Src and Fyn were unchanged. Densitometric analysis revealed an increase after haloperidol injection in the band of Tyr(P)-418 on Fyn but not Src. *D*, there was also a significant increase in the band density of Tyr(P)-1472 on NR2B following haloperidol injection in $+/fyn^Z$ mice. No such difference was detected in the fyn^Z/fyn^Z mice. The basal level of Tyr(P)-1472 in the fyn^Z/fyn^Z mice tended to decrease in comparison with the $+/fyn^Z$ mice, but the difference was not significant. The amount of NR2B was unchanged. *HAL*, haloperidol (1.0 mg/kg); *Veh*, vehicle. Four to six animals were used in each group. The *columns* represent means, and the *bars* represent means ± S.E. One-way ANOVA; *, $p < 0.01$; **, $p < 0.05$.

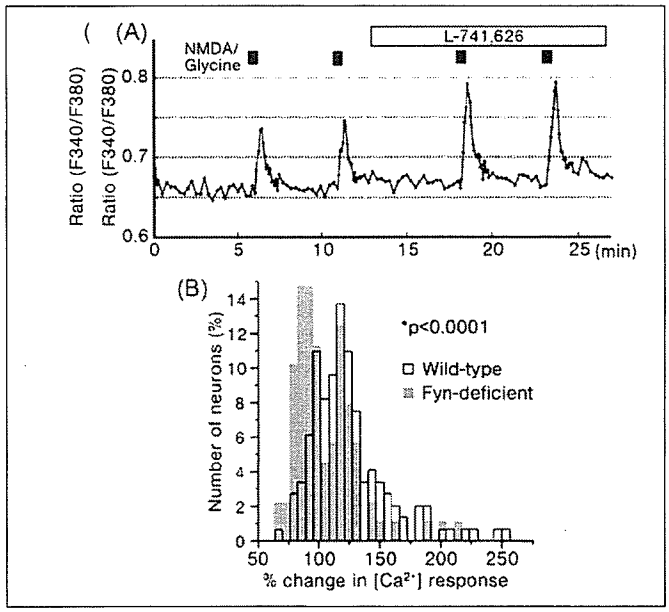

FIGURE 5. **Effect of a D_2-R selective antagonist, L-741,626, on the channel activity of NMDA receptors in primary striatal neurons assessed by Ca^{2+} fluorimetry.** *A*, $[Ca^{2+}]_i$ responses of wild-type neurons in the presence of quinpirole (50 μM). A representative trace of wild-type neurons exposed to two applications of 3 μM NMDA, 10 μM glycine (control response) and two applications of 3 μM NMDA, 10 μM glycine 5 min after starting L-741,626 (10 μM) addition to the perfusion buffer. The addition of L-741,626 significantly enhanced NMDA/glycine-induced $[Ca^{2+}]_i$ responses compared with the control responses. *B*, histogram of $[Ca^{2+}]_i$ responses induced by 3 μM NMDA, 10 μM glycine in the presence of L-741,626 (10 μM) relative to those in the absence of L-741,626 (control response). Large numbers (74.7%) of the wild-type neurons (*open bars*) exhibited larger NMDA/glycine-induced $[Ca^{2+}]_i$ responses after the addition of L-741,626 (mean change, 125.7 ± 34.1% of the control responses), whereas the number of Fyn-deficient neurons (*filled bars*) showing larger responses was significantly decreased (46.6%, mean change, 105.8 ± 26.9% of the control responses). There was also a group of Fyn-deficient neurons that exhibited larger responses after L-741,626 addition that peaked at around 120% of the control responses. Eight wild-type and six Fyn-deficient striatal neuronal cultures were used. Mann-Whitney *U* test.

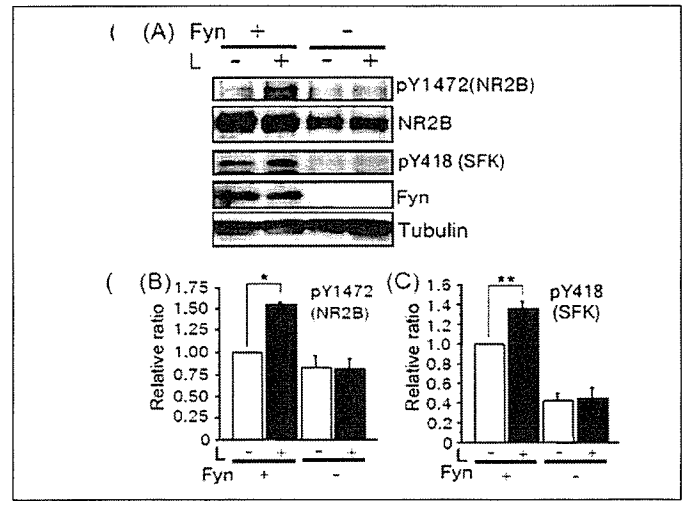

FIGURE 6. **Western blot analysis of striatal primary neurons.** *A*, neurons were exposed to or not exposed to L-741,626 (10 μM) in the presence of quinpirole. L-741,626 (10 μM) markedly increased the tyrosine phosphorylation at Tyr-1472 of NR2B (*pY1472*) and at Tyr-418 of Src family kinases (*pY418*) in the wild type, but no such difference was found in Fyn deficiency. *B*, densitometric analysis revealed a significant increase in the band density of the Tyr(P)-1472 of NR2B in the wild type. No such increase was detected in Fyn deficiency. *C*, there was also a significant increase in the band density of the Tyr(P)-418 of the Src family kinases when L-741,626 was added to the wild type. No such difference was detected in Fyn deficiency. Six wild-type and six Fyn-deficient striatal neuronal cultures were used. The *columns* represent means, and the *bars* represent S.E. One-way ANOVA; *, $p < 0.0001$; **, $p < 0.005$.

L-741,626, on the channel activity of NMDA receptors of wild-type neurons in the presence of a D_2-R-selective agonist, quinpirole (50 μM). After confirming that the responses evoked were reproducible by two successive applications of 3 μM NMDA, 10 μM glycine (control responses), we added 10 μM L-741,626 to the perfusion buffer BSS. After 5 min, we measured the 3 μM NMDA, 10 μM glycine-induced increases in $[Ca^{2+}]_i$ and compared them with the control responses. As shown in Fig. 5*A*, larger responses than the control responses were detected in the presence of L-741,626, but in some neurons, almost identical responses were observed both in the presence and absence (control) of L-741,626. The distribution of changes in $[Ca^{2+}]_i$ responses after the addition of L-741,626 is shown in Fig. 5*B* (*open bars*). After the addition of L-741,626, a large number of neurons (74.7%) showed larger responses than the control responses (mean change, 125.7 ± 34.1%).

To determine whether the larger NMDA/glycine-induced responses induced by L-741,626 were mediated by Fyn, we performed the same experiments on primary cultures prepared from Fyn-deficient mice. After the addition of L-741,626, only 46.6% of the Fyn-deficient neurons showed larger responses than the control responses, and L-741,626 addition had little enhancing effect on the responses (mean change, 106.8 ± 26.9% of the control responses; see Fig. 5*B*, *filled bars*). A subset of Fyn-deficient neurons exhibited larger responses after L-741,626 addition, and their responses peaked at around 120% of the control responses. In addition, the numbers of neurons exhibiting larger responses after L-741,626 addition was lower in the presence of the Src family inhibitor PP2 (10 μM) (mean change, 99.9 ± 15.7% of the control responses).

We then examined the effect of L-741,626 on Fyn activation and NMDA receptor phosphorylation in the presence of quinpirole (50 μM) by Western blot analysis, as shown in Fig. 6. Primary cells were exposed or not exposed (control) to 10 μM L-741,626 for 7 min prior to sample preparation. In the wild-type cells, immunoreactivity for anti-pY1472 antibody and anti-pY418 antibody in the L-741,626-treated cell extracts was stronger than in the control cell extracts. By contrast, when Fyn-deficient cells were used, there were no significant differences in immunoreactivity for anti-pY1472 antibody and anti-pY418 antibody between the L-741,626-exposed cell extracts and the control cell extracts.

DISCUSSION

The results of this study show that Fyn is required for haloperidol-induced catalepsy. We also found that haloperidol induces Fyn activation and a Fyn-dependent increase in NR2B phosphorylation in mouse striatum. We used striatal primary neurons to verify that D_2-R blockade induced Fyn activation, enhancement of NR2B phosphorylation, and potentiation of the channel activity of NMDA receptor at the cellular level, and the latter two effects were significantly reduced in Fyn-deficient neurons. On the basis of these findings, we propose a new molecular mechanism that underlies haloperidol-induced catalepsy in which the D_2-R antagonist induces Fyn activation in the striatum, and the subsequent phosphorylation of the NR2B subunit by the activated Fyn increases the channel activity of NMDA receptors, which leads to changes in neural transmission and results in the cataleptic response.

Because haloperidol-induced catalepsy and muscular rigidity are mainly caused by blockade of dopamine D_2-Rs in the striatum (1, 2), sensitivity to haloperidol should be altered by changes in dopaminergic transmission. However, there were no clear differences between Fyn-deficient mice and control mice in the expression pattern of the D_2-R gene or the amounts of D_2-R protein and tyrosine hydroxylase, and measurements by microdialysis showed no significant difference in striatal basal dopamine levels (32). Thus, it is rather unlikely that the

reduced sensitivity to haloperidol in the Fyn-deficient mice is because of defective dopaminergic transmission.

We found that haloperidol increased phosphorylation of the Tyr-418 residues of Fyn. The catalytic activity of SFKs is controlled through autocatalytic phosphorylation and dephosphorylation, particularly at amino acid residues Tyr-418 and Tyr-529 (14), and the phosphorylated Tyr-529 intramolecularly interacts with an Src homology 2 domain to form a loop, thereby suppressing kinase function. Intermolecular autophosphorylation at Tyr-418, on the other hand, activates SFKs by displacing Tyr-418 from the substrate-binding site, thus allowing the kinase to gain access to substrates (33). We found that the haloperidol-induced increase in Tyr-418 phosphorylation occurred specifically in Fyn and did not occur in Src, whereas phosphorylation of Tyr-529 was the same in both Src and Fyn. Thus, Fyn is specifically activated by haloperidol *in vivo*.

Haloperidol also increased the phosphorylation of Tyr-1472 in the NR2B subunit, and because no increase was observed in Fyn-deficient mice, the haloperidol-induced phosphorylation of NR2B subunit must be dependent on Fyn. Moreover, we confirmed this D_2-R antagonist induced Fyn-mediated enhancement of NR2B phosphorylation at the cellular level in primary cultures of striatal neurons.

Fyn-mediated phosphorylation of NR2B and potentiation of NMDA-R channel activity are involved in several brain functions, including ethanol tolerance (15), seizure susceptibility (23), and long term potentiation (17). Activation of EphB receptors has also been reported to result in increased phosphorylation of NR2B and an increase in NMDA-R channel activity measured by Ca^{2+} imaging in hippocampal primary cultures (34). The use of HEK293T cells transfected with a mutant NR2B construct in this study also showed that Fyn-mediated tyrosine phosphorylation of NR2B is required for the increase in NMDA-R channel activity. In our study, NMDA-R channel activity in most wild-type striatal neurons was increased by the blockade of D_2-R, and the proportion of such neurons was significantly reduced in Fyn deficiency. Thus, the increased NMDA-R activity after D_2-R blockade in most of the striatal neurons was Fyn-dependent. However, NMDA-R may also be activated by a Fyn-independent pathway, because a certain proportion of the neurons in the Fyn-deficient striatal culture exhibited increased NMDA-R activity.

It has been repeatedly observed that the NMDA-R antagonist MK-801 attenuates haloperidol-induced catalepsy (9, 35–37), and we recently reported that prior exposure to the NR2B-selective antagonist CP-101,606 significantly reduces haloperidol-induced catalepsy (9). Thus, haloperidol-induced catalepsy is specifically dependent on NR2B function, and activation of NR2B function by Fyn-mediated phosphorylation is likely to be required for catalepsy to occur.

NMDA-R dysfunction is hypothesized to be the pathogenetic mechanism responsible for schizophrenia, because NMDA-R antagonists cause psychotic states resembling schizophrenia (38–40), and mice with reduced NMDA-R expression have been reported to display schizophrenia-related behaviors (41). Because unmedicated schizophrenic patients exhibit attenuated EPS shortly after haloperidol administration compared with healthy controls (42), the lower responsiveness to haloperidol in Fyn-deficient mice may mimic a feature of schizophrenia.

Several mutant mice, including mice deficient in the D_2-R (24), A_{2A}-adenosine receptor (43), retinoid X receptor γ1 (44), and protein kinase A (PKA) (45), show reduced cataleptic responses to haloperidol. The reduced cataleptic response in one of them, the PKA-deficient mutant, is likely to be caused by a molecular mechanism similar to that in Fyn deficiency, because an increase in PKA-mediated serine phosphorylation of striatal NR1 subunits increases following haloperidol administration (46). The scaffolding protein RACK1 binds to both Fyn and NR2B, and the three molecules form a complex in rat hippocampus (16, 47). Dissociation of RACK1 from this RACK1-Fyn-NR2B complex facilitates Fyn-mediated phosphorylation of NR2B (47). Because PKA activation has been demonstrated to dissociate RACK1 from this complex (16), the above PKA-RACK1-Fyn pathway may also exist downstream of D_2-R in the striatum.

Another molecule that may act between D_2-R and Fyn is PKC. Activation of G-protein-coupled receptors, such as muscarinic and metabotropic glutamate receptors, in the hippocampus increases NMDA-evoked currents via protein kinase C (PKC) (48). The increase in NMDA-R function is mediated by the activation of SFKs, because the PKC-induced NMDA-R up-regulation is blocked by an inhibitor of Src and Fyn and does not occur in Src-deficient cells (48). D_2-R is another G-protein-coupled receptor, and because haloperidol administration acutely increases PKC activity in the rat striatum (49), Fyn activation after D_2-R blockade may be mediated by the PKC pathway.

Other molecules, including receptor tyrosine kinases (34, 50) and a cytokine receptor (51), have also been reported to be involved in SFK-mediated phosphorylation and activation of NMDA-R, and they may be involved in the striatal activation of Fyn after D_2-R inhibition.

In this study we found that blockade of D_2-R causes Fyn activation, Fyn-mediated NMDA-R phosphorylation, and potentiation of its channel activity in the striatal neurons that may be responsible for haloperidol-induced catalepsy. Further investigation should focus on the above-postulated Fyn-activation mechanisms initiated by D_2-R blockade, and these transduction steps should be drug targets for controlling not only motor function but higher cognitive brain function.

Acknowledgments—We are grateful to Dr. H. Niki (Brain Science Institute, RIKEN, Japan) for reading the manuscript and giving us invaluable advice. We are also grateful to Dr. T. Kaneko (Kyoto University) for the gift of the mouse dopamine D_2 receptor cDNA, Dr. M. Watanabe (Hokkaido University) for the gift of the anti-NR2B antibody, and Prof. N. Koshikawa (Department of Pharmacology, Nihon University School of Dentistry) for helpful advice on the determination of muscular rigidity. We also thank K. Kamimura and T. Muto (Department of Anatomy and Developmental Biology, Chiba University Graduate School of Medicine) for their technical assistance in the immunohistochemistry and behavioral analyses.

REFERENCES

1. Crocker, A. D., and Hemsley, K. M. (2001) *Prog. Neuropsychopharmacol. Biol. Psychiatry* **25,** 573–590
2. Wadenberg, M. L., Soliman, A., VanderSpek, S. C., and Kapur, S. (2001) *Neuropsychopharmacology* **25,** 633–641
3. Moore, N. A., Blackman, A., Awere, S., and Leander, J. D. (1993) *Eur. J. Pharmacol.* **237,** 1–7
4. Chartoff, E. H., Ward, R. P., and Dorsa, D. M. (1999) *J. Pharmacol. Exp. Ther.* **291,** 531–537
5. Chase, T. N. (2004) *Parkinsonism Relat. Disord.* **10,** 305–313
6. Sucher, N. J., Awobuluyi, M., Choi, Y. B., and Lipton, S. A. (1996) *Trends Pharmacol. Sci.* **17,** 348–355
7. Standaert, D. G., Testa, C. M., Young, A. B., and Penney, J. B., Jr. (1994) *J. Comp. Neurol.* **343,** 1–16
8. Kosinski, C. M., Standaert, D. G., Counihan, T. J., Scherzer, C. R., Kerner, J. A., Daggett, L. P., Velicelebi, G., Penney, J. B., Young, A. B., and Landwehrmeyer, G. B. (1998) *J. Comp. Neurol.* **390,** 63–74
9. Yanahashi, S., Hashimoto, K., Hattori, K., Yuasa, S., and Iyo, M. (2004) *Brain Res.* **1011,** 84–93
10. Wang, Y. T., and Salter, M. W. (1994) *Nature* **369,** 233–235
11. Tingley, W. G., Ehlers, M. D., Kameyama, K., Doherty, C., Ptak, J. B., Riley, C. T., and Huganir, R. L. (1997) *J. Biol. Chem.* **272,** 5157–5166
12. Menegoz, M., Lau, L. F., Herve, D., Huganir, R. L., and Girault, J. A. (1995) *Neuroreport* **7,** 125–128
13. Oh, J. D., Russell, D. S., Vaughan, C. L., Chase, T. N., and Russell, D. (1998) *Brain Res.* **813,** 150–159

14. Salter, M. W., and Kalia, L. V. (2004) *Nat. Rev. Neurosci.* **5,** 317–328
15. Miyakawa, T., Yagi, T., Kitazawa, H., Yasuda, M., Kawai, N., Tsuboi, K., and Niki, H. (1997) *Science* **278,** 698–701
16. Yaka, R., Phamluong, K., and Ron, D. (2003) *J. Neurosci.* **23,** 3623–3632
17. Nakazawa, T., Komai, S., Tezuka, T., Hisatsune, C., Umemori, H., Semba, K., Mishina, M., Manabe, T., and Yamamoto, T. (2001) *J. Biol. Chem.* **276,** 693–699
18. Kojima, N., Ishibashi, H., Obata, K., and Kandel, E. R. (1998) *Learn. Mem.* **5,** 429–445
19. Cheung, H. H., and Gurd, J. W. (2001) *J. Neurochem.* **78,** 524–534
20. Yagi, T., Shigetani, Y., Okado, N., Tokunaga, T., Ikawa, Y., and Aizawa, S. (1993) *Oncogene* **8,** 3343–3351
21. Kulagowski, J. J., Broughton, H. B., Curtis, N. R., Mawer, I. M., Ridgill, M. P., Baker, R., Emms, F., Freedman, S. B., Marwood, R., Patel, S., Ragan, C. I., and Leeson, P. D. (1996) *J. Med. Chem.* **39,** 1941–1942
22. Watanabe, M., Fukaya, M., Sakimura, K., Manabe, T., Mishina, M., and Inoue, Y. (1998) *Eur. J. Neurosci.* **10,** 478–487
23. Yasunaga, M., Yagi, T., Hanzawa, N., Yasuda, M., Yamanashi, Y., Yamamoto, T., Aizawa, S., Miyauchi, Y., and Nishikawa, S. (1996) *J. Cell Biol.* **132,** 91–99
24. Boulay, D., Depoortere, R., Oblin, A., Sanger, D. J., Schoemaker, H., and Perrault, G. (2000) *Eur. J. Pharmacol.* **391,** 63–73
25. Lorenc-Koci, E., Wolfarth, S., and Ossowska, K. (1996) *Exp. Brain Res.* **109,** 268–276
26. Yuasa, S. (1996) *Anat. Embryol.* **194,** 223–234
27. Uchino, S., Watanabe, W., Nakamura, T., Shuto, S., Kazuta, Y., Matsuda, A., Nakajima-Iijima, S., Kudo, Y., Kohsaka, S., and Mishina, M. (2001) *FEBS Lett.* **506,** 117–122
28. Cepeda, C., Buchwald, N. A., and Levine, M. S. (1993) *Proc. Natl. Acad. Sci. U. S. A.* **90,** 9576–9580
29. Millan, M. J., Dekeyne, A., Rivet, J. M., Dubuffet, T., Lavielle, G., and Brocco, M. (2000) *J. Pharmacol. Exp. Ther.* **293,** 1063–1073
30. Miyakawa, T., Yagi, T., Kagiyama, A., and Niki, H. (1996) *Brain Res. Mol. Brain Res.* **37,** 145–150
31. Miyakawa, T., Yagi, T., Watanabe, S., and Niki, H. (1994) *Brain Res. Mol. Brain Res.* **27,** 179–182
32. Hironaka, N., Yagi, T., and Niki, H. (2002) *Brain Res. Mol. Brain Res.* **98,** 102–110
33. Xu, W., Doshi, A., Lei, M., Eck, M. J., and Harrison, S. C. (1999) *Mol. Cell* **3,** 629–638
34. Takasu, M. A., Dalva, M. B., Zigmond, R. E., and Greenberg, M. E. (2002) *Science* **295,** 491–495
35. de Souza, I. E., and Meredith, G. E. (1999) *Synapse* **32,** 243–253
36. Dragunow, M., Robertson, G. S., Faull, R. L., Robertson, H. A., and Jansen, K. (1990) *Neuroscience* **37,** 287–294
37. Ziolkowska, B., and Hollt, V. (1993) *Neurosci. Lett.* **156,** 39–42
38. Olney, J. W., and Farber, N. B. (1995) *Arch. Gen. Psychiatry* **52,** 998–1007
39. Tsai, G., and Coyle, J. T. (2002) *Annu. Rev. Pharmacol. Toxicol.* **42,** 165–179
40. Svensson, T. H. (2000) *Brain Res. Brain Res. Rev.* **31,** 320–329
41. Mohn, A. R., Gainetdinov, R. R., Caron, M. G., and Koller, B. H. (1999) *Cell* **98,** 427–436
42. Miller, A. L., Maas, J. W., Contreras, S., Seleshi, E., True, J. E., Bowden, C., and Castiglioni, J. (1993) *Biol. Psychiatry* **34,** 178–187
43. Chen, J. F., Moratalla, R., Impagnatiello, F., Grandy, D. K., Cuellar, B., Rubinstein, M., Beilstein, M. A., Hackett, E., Fink, J. S., Low, M. J., Ongini, E., and Schwarzschild, M. A. (2001) *Proc. Natl. Acad. Sci. U. S. A.* **98,** 1970–1975
44. Saga, Y., Kobayashi, M., Ohta, H., Murai, N., Nakai, N., Oshima, M., and Taketo, M. M. (1999) *Genes Cells* **4,** 219–228
45. Adams, M. R., Brandon, E. P., Chartoff, E. H., Idzerda, R. L., Dorsa, D. M., and McKnight, G. S. (1997) *Proc. Natl. Acad. Sci. U. S. A.* **94,** 12157–12161
46. Leveque, J. C., Macias, W., Rajadhyaksha, A., Carlson, R. R., Barczak, A., Kang, S., Li, X. M., Coyle, J. T., Huganir, R. L., Heckers, S., and Konradi, C. (2000) *J. Neurosci.* **20,** 4011–4020
47. Yaka, R., Thornton, C., Vagts, A. J., Phamluong, K., Bonci, A., and Ron, D. (2002) *Proc. Natl. Acad. Sci. U. S. A.* **99,** 5710–5715
48. Lu, W. Y., Xiong, Z. G., Lei, S., Orser, B. A., Dudek, E., Browning, M. D., and MacDonald, J. F. (1999) *Nat. Neurosci.* **2,** 331–338
49. Dwivedi, Y., and Pandey, G. N. (1999) *J. Pharmacol. Exp. Ther.* **291,** 688–704
50. Kotecha, S. A., Oak, J. N., Jackson, M. F., Perez, Y., Orser, B. A., Van Tol, H. H., and MacDonald, J. F. (2002) *Neuron* **35,** 1111–1122
51. Viviani, B., Bartesaghi, S., Gardoni, F., Vezzani, A., Behrens, M. M., Bartfai, T., Binaglia, M., Corsini, E., Di Luca, M., Galli, C. L., and Marinovich, M. (2003) *J. Neurosci.* **23,** 8692–8700

Journal of Neurochemistry, 2006, **97**, 1203–1214 doi:10.1111/j.1471-4159.2006.03831.x

Direct interaction of post-synaptic density-95/Dlg/ZO-1 domain-containing synaptic molecule Shank3 with GluR1 α-amino-3-hydroxy-5-methyl-4-isoxazole propionic acid receptor

Shigeo Uchino, Hidenori Wada, Shizuyo Honda, Yasuko Nakamura, Yumiko Ondo, Takayoshi Uchiyama, Moe Tsutsumi, Eri Suzuki, Takae Hirasawa and Shinichi Kohsaka

Department of Neurochemistry, National Institute of Neuroscience, Kodaira, Tokyo, Japan

Abstract

A class of scaffolding protein containing the post-synaptic density-95/Dlg/ZO-1 (PDZ) domain is thought to be involved in synaptic trafficking of α-amino-3-hydroxy-5-methyl-4-isoxazole propionic acid (AMPA) receptors during development. To clarify the molecular mechanism of AMPA receptor trafficking, we performed a yeast two-hybrid screening system using the cytoplasmic tail of the GluR1 subunit of AMPA receptor as a bait and identified a synaptic molecule, Shank3/ProSAP2, as a GluR1 subunit-interacting molecule. Shank3 is a PDZ domain-containing multidomain protein and is predominantly expressed in developing neurons. Using the glutathione S-transferase pull-down assay and immunoprecipitation technique we demonstrated that the GluR1 subunit directly binds to the PDZ domain of Shank3 via its carboxyl terminal PDZ-binding motif. We raised anti-Shank3 antibody to investigate the expression of Shank3 in cortical neurons. The pattern of Shank3 immunoreactivity was strikingly punctate, mainly observed in the spines, and closely matched the pattern of post-synaptic density-95 immunoreactivity, indicating that Shank3 is colocalized with post-synaptic density-95 in the same spines. When Shank3 and the GluR1 subunit were overexpressed in primary cortical neurons, they were also colocalized in the spines. Taken together with the biochemical interaction of Shank3 with the GluR1 subunit, these results suggest that Shank3 is an important molecule that interacts with GluR1 AMPA receptor at synaptic sites of developing neurons.

Keywords: α-amino-3-hydroxy-5-methyl-4-isoxazole propionic acid receptor, development, GluR1 subunit, post-synaptic density-95/ Dlg/ ZO-1 domain, Shank3, synapse.

J. Neurochem. (2006) **97**, 1203–1214.

Transmission at excitatory synapses is primarily mediated by glutamate acting on three classes of ligand-gated ion channels, α-amino-3-hydroxy-5-methyl-4-isoxazole propionic acid (AMPA), kainate and NMDA receptors (Wisden and Seeburg 1993; Hollmann and Heinemann 1994). In addition to their role in synaptic transmission, these glutamate receptors (GluRs) have been thought to play a crucial role in many brain functions, including activity-dependent synaptogenesis during development and synaptic plasticity (McDonald and Johnston 1990; Bliss and Collingridge 1993).

Many excitatory synapses in young developing neurons have been found to express only NMDA receptors, which are continuously blocked by magnesium at resting membrane potentials. As no evoked transmission is observed even when glutamate is present, these synapses are referred to as 'silent synapses'. During later development, AMPA receptors are delivered and clustered on the synaptic membrane in an activity-dependent manner, and the synapses subsequently become functionally active (Durand *et al.* 1996; Wu *et al.* 1996; Pickard *et al.* 2000; Liao *et al.* 2001; Isaac 2003). Thus, the clustering of AMPA receptors on the synaptic membrane is an essential event during synaptogenesis.

Received November 16, 2005; revised manuscript received February 2, 2006; accepted February 9, 2006.

Address correspondence and reprint requests to S. Kohsaka, Department of Neurochemistry, National Institute of Neuroscience, 4-1-1 Ogawahigashi, Kodaira, Tokyo 187-8502, Japan.
E-mail: kohsaka@ncnp.go.jp

Abbreviations used: aa, amino acid; AMPA, α-amino-3-hydroxy-5-methyl-4-isoxazole propionic acid; EGFP, enhanced green fluorescent protein; EGFP-GluR1, enhanced green fluorescent protein-fused GluR1 subunit; GluR, glutamate receptor; GST, glutathione S-transferase; mShank3, mouse Shank3; NR2B, NMDA receptor 2B; PBS, phosphate-buffered saline; PDZ, post-synaptic density-95/Dlg/ZO-1; PFA, paraformaldehyde; PSD-95, post-synaptic density-95; SAP-97, synapse-associated protein 97; SDS, sodium dodecyl sulfate; SH3, Src homology 3.

The AMPA receptors are heteromeric complexes of four homologous subunits, GluR1–GluR4 (Wisden and Seeburg 1993; Hollmann and Heinemann 1994). The expression of GluR1–GluR3 subunits increases during development, whereas the expression of GluR4 subunit is seen in earlier development (Zhu *et al.* 2000). Recent studies have shown that induction of long-term potentiation or activation of Ca^{2+}/calmodulin-dependent protein kinase II promoted delivery of GluR1 subunit-containing AMPA receptors to synapses, and that this effect was diminished by mutating the post-synaptic density-95 (PSD-95)/Dlg/ZO-1 (PDZ) domain binding motif at the C-terminal end of the GluR1 subunit (Shi *et al.* 1999; Hayashi *et al.* 2000). This finding indicates that PDZ domain-containing proteins participate in regulating the synaptic localization of GluR1 subunit-containing AMPA receptors; however, this protein remains to be identified. So far, biochemical analysis has shown that GluR1 subunit binds to synapse-associated protein 97 (SAP-97) via its C-terminal PDZ-binding motif (Leonard *et al.* 1998). In developing neurons, however, expression of SAP-97 is distributed more in the somatic region than in the synapses. Thus, SAP-97 is thought to be associated with intracellular AMPA receptors, including GluR1 subunit, and to be involved in the early secretory pathway of AMPA receptor trafficking (Sans *et al.* 2001).

In this study, we used a yeast two-hybrid screening system to search for the protein that interacts with the PDZ-binding motif of GluR1 AMPA receptor, and we identified Shank3/ProSAP2 from the mouse brain cDNA library. Shank3 is a multidomain protein that contains ankyrin repeats, a Src homology 3 (SH3) domain, a PDZ domain, a long proline-rich region and a sterile alpha motif, and is predominantly expressed in spines during synaptogenesis (Lim *et al.* 1999; Naisbitt *et al.* 1999; Sheng and Kim 2000; Böckers *et al.* 2001, 2002). In the present study we found that Shank3 biochemically interacts with the PDZ-binding motif of GluR1 subunit and that Shank3 is colocalized with GluR1 AMPA receptor in the spines. These findings suggest that Shank3 is a candidate clue molecule for clarifying the molecular mechanism of AMPA receptor trafficking to synapses during synaptogenesis.

Materials and methods

Yeast two-hybrid screening

The cDNA fragment encoding the C-terminal 81-amino-acid segment [amino acids (aa) 809–889] of mouse GluR1 subunit was inserted into pLexA to yield a bait plasmid, pLexA-GluR1/C. The bait plasmid was transformed with yeast strain L40 and a mouse brain cDNA library (Clontech, Palo Alto, CA, USA) was used to screen for proteins that interacted with LexA-GluR1/C fusion proteins. Interactions were detected by induction of reporter genes, *HIS3*, *TRP1*, *LUE2* and *LacZ*, which resulted in cell growth and the formation of blue colonies on histidine-, tryptophan- and leucine-depleted yeast synthetic media containing X-gal (80 μg/mL).

Plasmid construction cDNA fragments encoding the full-length mouse Shank3 (mShank3; aa 1–1730), the SH3 and PDZ domains of mShank3 (mShank3/SH3-PDZ; aa 461–671), the PDZ domain (mShank3/PDZ; aa 552–671), the C-terminal fragment containing the PDZ domain (mShank3/PDZ + C; aa 552–1730) and the C-terminal fragment without the PDZ domain (mShank3/C; aa 670–1730) were constructed by PCR and subcloned into a mammalian expression vector, pCMV-Myc (Clontech), to obtain pCMV-myc-mShank3, pCMV-myc-mShank3/SH3-PDZ, pCMV-myc-mShank3/PDZ, pCMV-myc-mShank3/PDZ + C and pCMV-myc-mShank3/C, respectively. Fusion proteins of the regions of mShank3, GluR1 subunit and mouse NMDA receptor 2B (NR2B) (GluRε2) subunit with glutathione S-transferase (GST) (and myc) were constructed by subcloning PCR-amplified DNA fragments into pGEX-4T-2 (Amersham, Piscataway, NJ, USA) containing a thrombin cleavage site or into pGEX-5X-2 (Amersham) containing a factor Xa cleavage site to obtain: pGEX-4T-2, pGEX-mShank3/SH3-PDZ (aa 461–671), pGEX-mShank3/SH3 (aa 461–551), pGEX-mShank3/PDZ (aa 552–671), pGEX-myc-mShank3/SH3-PDZ (aa 461–671), pGEX-GluR1/C (aa 809–889), pGEX-GluR1/del (deletion of four aa from the C-terminal end) (aa 809–885), pGEX-GluR1/mu (exchange of four aa in the C-terminal end, ATGL to AAGA), pGEX-C-terminal segment of NR2B (aa 1279–1456), pGEX-5X-2 and pGEX-5X-GluR1/C (aa 809–889). All of the constructs were confirmed by DNA sequencing.

Cell culture and DNA transfection

Chinese hamster ovary cells or COS7 cells were grown at 37°C in a humidified 5% CO_2 atmosphere in Dulbecco's modified Eagle's medium (Gibco BRL, Grand Island, NY, USA) containing 10% heat-inactivated fetal bovine serum (Irvine, Santa Ana, CA, USA). For the transient expression studies, the cells were transfected with expression vector by using Lipofectamine Plus (Invitrogen, Carlsbad, CA, USA) according to the manufacturer's protocol.

Embryonic day 15–16 mouse cortical primary neurons were prepared as described previously (Hirasawa *et al.* 2003). Briefly, cerebral cortices were dissected, minced and dissociated with a papain. The dissociated cells were plated onto 0.1% polyethylenimine-coated plates at a density of $1.0–1.5 \times 10^4$ cells/cm^2 for immunocytochemistry and 1.0×10^5 cells/cm^2 for pull-down assays, and maintained in Neurobasal medium (Gibco BRL) containing 2% B-27 supplement (Gibco BRL) and 0.5 mM glutamine at 37°C under a humidified 10% CO_2 atmosphere for the periods indicated. For the transient expression studies, the cells were transfected with expression vector by using Lipofectamine 2000 (Invitrogen) according to the manufacturer's protocol.

The experimental protocols were approved by The Animal Care and Use Committee of the National Institute of Neuroscience.

Purification of recombinant proteins and pull-down assay

The GST fusion proteins were expressed in *Escherichia coli* BL21 and purified on glutathione sepharose 4B (Amersham) according to the manufacturer's protocol. The pull-down assay was performed essentially as described previously (Tu *et al.* 1999). Briefly, the Chinese hamster ovary cells transfected with myc-tagged protein or mouse cortical primary cells were lysed at 4°C for 1 h with a buffer

composed of 50 mM Tris-HCl (pH 7.5), 100 mM NaCl, 1 mM EDTA, protease inhibitor cocktail (Roche, Penzberg, Germany) and 0.1% Triton X-100 (for Chinese hamster ovary cells) or 1% Triton X-100 (for primary cultured cells). After removing the insoluble material by centrifugation (15 000 *g* for 20 min at 4°C), the protein concentration in the supernatant was determined with a protein assay kit (Pierce, Rockford, IL, USA). Soluble extracts were incubated for 12 h at 4°C with purified GST fusion protein bound to 20 μL of glutathione sepharose in phosphate-buffered saline (PBS) containing 0.1% Triton X-100 and protease inhibitor cocktail. The sepharose suspensions were washed four times with lysis buffer. Bound proteins were eluted by boiling in sodium dodecyl sulfate (SDS) sample buffer, separated by SDS–polyacrylamide gel electrophoresis and analysed by immunoblot.

Immunoprecipitation assay

COS7 cells were transfected with each of the expression vectors. At 2 days after transfection, cells were lysed at 4°C for 1 h with immunoprecipitation (IP) buffer composed of 50 mM Tris-HCl (pH 7.5), 150 mM NaCl, 0.5 mM EDTA, 10% glycerol, 0.5% Triton X-100 and protease inhibitor cocktail. After removing the insoluble material by centrifugation (15 000 *g* for 20 min at 4°C), the protein concentration in the supernatant was determined with a protein assay kit. Soluble extracts were incubated at 4°C for 2 h with rabbit polyclonal anti-enhanced green fluorescent protein (EGFP) antibody bound to protein A- and G-Sepharose beads (Amersham). The immunoprecipitates were washed three times with IP buffer, eluted by boiling in SDS sample buffer, separated by SDS–polyacrylamide gel electrophoresis and analysed by immunoblot.

Antibody production

Rabbit polyclonal antibody against a GST-fused mShank3 fragment (aa 1016–1357) was produced by Biotest Inc. (Tokyo, Japan).

Preparation of the synaptosomal fraction

The synaptosomal fraction was prepared essentially according to the procedures described previously (Carlin *et al.* 1980). In brief, cortex was dissected from mouse at 2 weeks of age and homogenized in 10 volumes of solution A (0.32 M sucrose, 1 mM $NaHCO_3$, 1 mM $MgCl_2$ and 0.5 M $CaCl_2$) with a Teflon homogenizer. The homogenate was centrifuged (1400 *g* for 10 min at 4°C) and the supernatant was saved. The pellet was suspended in solution A and centrifuged (700 *g* for 10 min at 4°C). The supernatants were pooled and then centrifuged (13 800 *g* for 10 min at 4°C). The resulting pellet was resuspended in solution B (0.32 M sucrose and 1 mM $NaHCO_3$), layered onto a discontinuous sucrose gradient containing 0.8 M/1.0 M/1.2 M sucrose and centrifuged (82 500 *g* for 2 h at 4°C). The fraction at the 1.0 M/1.2 M sucrose interface was isolated as the synaptosomal fraction and the protein concentration was determined with a protein assay kit.

Immunoblot analysis

The proteins were separated by electrophoresis through an SDS polyacrylamide gel (Daiichi Pure Chemicals, Tokyo, Japan) and then electrophoretically transferred to nitrocellulose membranes (Schleicher & Schuell, Dassel, Germany). The membranes were blocked by incubation for 1 h at room temperature (15~25°C) with 5% skim milk (Becton Dickinson, Sparks, MD, USA) in buffer A (10 mM Tris-HCl, pH 7.5, 100 mM NaCl and 0.1% Tween 20) and then incubated for 1 h at room temperature with one of the following primary antibodies in buffer A containing 3% skim milk: rabbit polyclonal anti-mShank3 antibody (0.1 μg/mL), mouse monoclonal anti-myc antibody (1 : 1000; Roche), mouse monoclonal anti-PSD-95 antibody (1 : 200; Affinity Bioreagents Inc., Golden, CO, USA), rabbit polyclonal anti-GluR1 antibody (1 : 200; Chemicon, Temecula, CA, USA), rabbit polyclonal anti-GluR2 antibody (1 : 200; Chemicon) or rabbit polyclonal anti-EGFP antibody (1 : 1000; Molecular Probes, Eugene, OR, USA). After three washes in buffer A, the membranes were incubated for 1 h at room temperature with horseradish peroxidase-conjugated anti-rabbit IgG secondary antibody (1 : 1000; Amersham) or horseradish peroxidase-conjugated anti-mouse IgG secondary antibody (1 : 1000; Amersham) and washed three times with buffer A. Immunoreactive bands were visualized with a chemiluminescence detection system (ECL; Amersham).

Preparation of membrane fraction and coimmunoprecipitation assay

To prepare the membrane fraction, the cortex was dissected from mouse at 2 weeks of age and homogenized with a Teflon homogenizer in PBS containing 0.25 M sucrose and protease inhibitor cocktail. The homogenate was centrifuged at 2000 *g* for 10 min to remove nuclei and debris, at 8000 *g* for 30 min to remove mitochondria and then at 100 000 *g* for 1 h to obtain the pellet as membrane fraction. The membrane proteins were solubilized at 4°C for 2 h with 2% SDS in PBS containing protease inhibitor cocktail and then diluted with five volumes of 2% Triton-X-100 in PBS as described in the previous study in which the binding of Kir 2.3 and PSD-95 was confirmed (Cohen *et al.* 1996). They were subsequently incubated at 4°C for 2 h with rabbit polyclonal anti-Shank3 antibody bound to protein A- and G-Sepharose beads. The immunoprecipitates were washed three times with IP buffer composed of 50 mM Tris-HCl (pH 7.5), 150 mM NaCl, 0.5 mM EDTA, 10% glycerol, 0.5% Triton X-100 and protease inhibitor cocktail, eluted by boiling in SDS sample buffer, separated by SDS–polyacrylamide gel electrophoresis and analysed by immunoblot.

Immunocytochemistry

Primary cells were fixed with 2% paraformaldehyde (PFA) for 10 min at room temperature. After three washes in PBS, the cells were permeabilized and blocked with 3% goat serum/0.1% Triton X-100 in PBS for 15 min, and then incubated for 1 h at room temperature with one of the following primary antibodies in PBS containing 3% bovine serum albumin (Sigma, St Louis, MO, USA): rabbit polyclonal anti-mShank3 antibody (1.0 μg/mL), mouse monoclonal anti-PSD-95 antibody (1 : 200), mouse monoclonal anti-myc antibody (1 : 500) or rabbit polyclonal anti-EGFP antibody (1 : 500). After three washes in PBS, the cells were incubated for 1 h at room temperature with Alexa Fluor 488 goat anti-mouse IgG (H + L) (1 : 1000; Molecular Probes), Alexa Fluor 488 goat anti-rabbit IgG (H + L) (1 : 1000; Molecular Probes), Alexa Fluor 594 goat anti-mouse IgG (H + L) (1 : 1000; Molecular Probes) or Alexa Fluor 594 goat anti-rabbit IgG (H + L) (1 : 1000; Molecular Probes) in PBS containing 3% bovine serum albumin. After three washes in PBS, the cells were mounted on a glass slide with PermaFluor (Thermo Shandon, Pittsburgh, PA, USA) containing

10% FluoroGuard (Bio-Rad, Hercules, CA, USA) to inhibit photobleaching and examined with a fluorescence microscope (AX70; Olympus, Tokyo, Japan). For surface staining of EGFP-fused GluR1 subunit (EGFP-GluR1), cells were first incubated for 20 min at room temperature with rabbit polyclonal anti-EGFP antibody (1 : 500) in PBS and, after washing in PBS, they were incubated for 20 min at room temperature with Alexa Fluor 488 goat anti-rabbit IgG (H + L) (1 : 1000) in PBS and fixed with 2% PFA for 10 min. They were then permeabilized and blocked for 15 min with 3% goat serum/0.1% Triton X-100 in PBS for subsequent immunostaining.

In situ hybridization

Three cDNA fragments (620 bp, 650 bp and 1 kb) of the unique region of mShank1, mShank2 and mShank3, respectively, were obtained by PCR and subcloned into mammalian expression vector pCMV-SPORT (Gibco BRL). Sense and antisense digoxigenin-labeled probes were produced with SP6 and T7 polymerase, respectively.

Brain specimens were prepared from mice as follows. Anesthetized mice were transcardially perfused with 4% PFA in PBS. Their brains were removed from the skulls and immersed in 4% PFA at 4°C for 2 days, and then in 30% sucrose at 4°C for 2 days. After embedding in optimal cutting temperature compound (Sakura Finetechnical Co. Ltd, Tokyo, Japan), they were quickly frozen in dry ice. Frozen brain sections (14 μm thick) were cut in the sagittal plane with a cryostat (CM-3000; Leica, Nussloch, Germany) and the sections were mounted on 3-aminopropyltriethoxysilane-coated glass slides (Matsunami, Osaka, Japan) and stored at − 80°C until use.

For hybridization, the sections were treated with 4 μg/mL pepsin/0.2 N HCl for 2 min at 37°C, washed twice in PBS containing 0.1% Tween 20 and post-fixed with 4% PFA for 30 min. After washing in PBS containing 0.1% Tween 20 for 5 min, the sections were treated with 0.2% diethylpyrocarbonate in PBS containing 0.1% Tween 20 and hybridized at 65°C for 16 h with 10 μg/mL digoxigenin-labeled probe in a buffer composed of 50% formamide, 5× saline sodium citrate, 1% SDS, 50 μg/mL heparin and 50 μg/mL yeast RNA. They were then washed for 30 min at 65°C in 5× saline sodium citrate containing 50% formamide and 1% SDS, and then twice for 45 min at 65°C in 2× saline sodium citrate containing 50% formamide. After washing in TBS-T (136 mM NaCl, 2.7 mM KCl, 250 mM Tris-HCl, pH 7.5, 0.1% Tween 20) for 20 min at room temperature, they were blocked with 0.2% blocking reagent (Roche) for 40 min and incubated with alkaline phosphatase-conjugated anti-digoxigenin Fab fragments (1 : 2000; Roche) diluted in blocking solution at 4°C for 16 h. They were then washed in TBS-T for 20 min at room temperature and alkaline phosphatase-conjugated antibody was visualized by reaction with 35 μg/mL 4-nitroblue tetrazolium chloride/17.5 μg/mL 5-bromo-4-chloro-3-indolyl-phosphate (Roche) in 100 mM Tris-HCl (pH 9.5), 100 mM NaCl, 50 mM $MgCl_2$, 0.1% Tween 20 and 2 mM levamisole (Sigma) at room temperature for 1–2 nights in the dark. The color reaction was stopped with deionized water and the sections were dehydrated in a graded ethanol series and mounted with Entellan (Merck, Darmstadt, Germany).

RT-PCR

Total RNA was extracted from mouse cortex with acid guanidinium thiocyanate-phenol-chloroform (Chomczynski and Sacchi 1987) and RT-PCR was performed by using an Advantage RT for PCR kit (Clontech) according to the manufacturer's protocol. The thermocycle profile for PCR amplification was: 30 s at 95°C, 30 s at 55°C, 1 min at 72°C for 30 cycles (mShank1), 33 cycles (mShank2 and mShank3) or 22 cycles (glyceraldehyde-3-phosphate dehydrogenase used as an internal control). The PCR products were separated on a 3% agarose gel and stained with ethidium bromide. The gel images were fed into an image processor (Archiver Eclipse; Fotodyne, Hartland, WI, USA) and quantitatively analysed with NIH imaging software. The primers for PCR analysis were: for mShank1, forward GGCAGGCGTAGGAAGCTCTA and reverse CTCATCCATGTCTGGGTG; for mShank2, forward TATGATGAGCGTCCCCGGCGG and reverse ATCATCAGGGTCTAGATT; for mShank3, forward GGCCCGAAGCGGAAACTTT and reverse ACCATCCTCCTCGGGTTT; and for glyceraldehyde-3-phosphate dehydrogenase, forward GTCATCATCTCCGCCCCTTCTGC and reverse GATGCCTGCTTCACCACCTTCTTG.

Results

Screening for proteins that interact with GluR1 subunit of α-amino-3-hydroxy-5-methyl-4-isoxazole propionic acid receptor

We used a yeast two-hybrid method to identify proteins that interact with GluR1 subunit of AMPA receptor. Using the C-terminal 81-amino-acid segment of GluR1 subunit as yeast two-hybrid bait, we identified several clones from among approximately 1×10^7 mouse brain clones. Sequencing analysis revealed that one of them, clone 321, encoded the C-terminal 1305-amino-acid segment of Shank3, which includes the SH3 and PDZ domains (Fig. 1a). We then cloned full-length Shank3 cDNA from mouse brain by RT-PCR. The deduced mShank3 protein showed 98% sequence identity with rat Shank3.

Shank3 is a multidomain protein that contains ankyrin repeats, an SH3 domain, a PDZ domain, a long proline-rich region and a sterile alpha motif (Fig. 1a), and it scaffolds various proteins, including guanylate kinase-associated protein (GKAP) and Homer, in excitatory post-synapses (Naisbitt *et al.* 1999; Sheng and Kim 2000; Böckers *et al.* 2001). We initially focused on the SH3 and PDZ domains of mShank3, as they are important for interaction with proteins. We investigated the biochemical interaction between mShank3 and GluR1 subunit by GST pull-down assay using the GST-fused SH3 and PDZ domains of mShank3 (GST-mShank3/SH3-PDZ) and extracts from mouse cortical primary cells. GST-mShank3/SH3-PDZ clearly pulled down GluR1 subunit, indicating that mShank3 binds to GluR1 subunit through the SH3-PDZ domains (Fig. 1b). In addition, we examined the other synaptic molecules, GluR2 subunit of AMPA receptor and PSD-95. As shown in Fig. 1(b), GST-mShank3/SH3-PDZ pulled down PSD-95 but not GluR2 subunit.

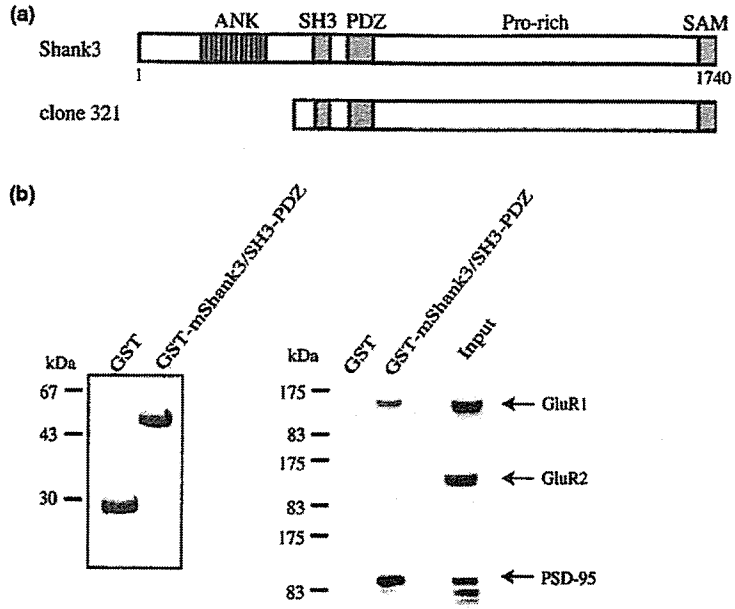

Fig. 1 Schematic structure of Shank3 and the biochemical interaction of mouse Shank3 (mShank3) with GluR1 subunit. (a) The schematic structure of Shank3 and clone 321. ANK, Ankyrin repeats 1–7; SH3, Src homology 3 domain; PDZ, post-synaptic density-95/Dlg/ZO-1 domain; SAM, sterile alpha motif. (b) Pull-down assay. The left panel shows the purified glutathione S-transferase (GST) and GST-fused mShank3/SH3-PDZ separated by sodium dodecyl sulfate–polyacrylamide gel electrophoresis (SDS–PAGE), and the right panel shows the immunoblots. GST alone or GST-fused mShank3/SH3-PDZ bound to glutathione sepharose beads was incubated with 1 mg of extract from mouse cortical primary cells cultured for 14 days. After washing, the proteins on the beads were eluted with SDS–PAGE sample buffer and immunoblotted with anti-GluR1 antibody, anti-GluR2 antibody or anti-post-synaptic density-95 (PSD-95) antibody. The input lane was loaded with 25 μg of the primary cell extract. Molecular weight standards are shown on the left.

Post-synaptic density-95/Dlg/ZO-1 domain of mouse Shank3 directly binds to the C-terminal segment of GluR1 subunit

To identify the interactive domain of mShank3, we constructed GST-mShank3/SH3, GST-mShank3/PDZ and GST-mShank3/SH3-PDZ (Fig. 2a), and performed a GST pull-down assay using cell lysates of Chinese hamster ovary cells expressing the myc-tagged C-terminal 81-amino-acid segment of GluR1 (myc-GluR1/C). As shown by SDS–polyacrylamide gel electrophoresis (Fig. 2a), the concentrations of each of the purified GST fusion proteins were almost the same. GST-mShank3/SH3-PDZ and GST-mShank3/PDZ clearly pulled down myc-GluR1/C, whereas no binding of GST-mShank3/SH3 to myc-GluR1/C was detected (Fig. 2a). These results suggest that GluR1 interacts with mShank3 via the PDZ domain.

We next investigated whether the interaction between mShank3/SH3-PDZ and GluR1/C was direct. The GST-fused myc-tagged SH3-PDZ domain of mShank3 (GST-myc-mShank3/SH3-PDZ) was expressed in *E. coli* BL21. After purification with glutathione sepharose, thrombin was reacted at 37°C for 1 h with the GST-myc-mShank3/SH3-PDZ bound to glutathione sepharose beads in PBS and purified myc-tagged mShank3/SH3-PDZ was obtained. GST-GluR1/C was produced using pGEX-5X-2 vector to protect against thrombin digestion and pull-down assays were performed. As shown in Fig. 2(b), purified myc-mShank3/SH3-PDZ bound to GST-GluR1/C, indicating that mShank3/SH3-PDZ binds directly to GluR1/C.

GluR1 subunit binds to the post-synaptic density-95/Dlg/ZO-1 domain of mouse Shank3 through its C-terminal post-synaptic density-95/Dlg/ZO-1 binding motif

As the C-terminal sequence of GluR1 subunit, -ATGL, is a typical PDZ-binding motif, -X-T/S-X-V/L/I (X represents any aa) (Songyang *et al.* 1997), we investigated whether the interaction between the PDZ domain of mShank3 and GluR1 subunit is mediated by the PDZ-binding motif of GluR1 subunit. To precisely identify the C-terminal residues involved in the binding, we prepared mutated GluR1/C carrying AAGA residues instead of ATGL and deleted GluR1/C lacking ATGL residues at its C-terminal end (Fig. 3a), and binding of these GluR1/C mutants to myc-mShank3/SH3-PDZ was almost abolished (Fig. 3b). The NR2B subunit, which binds to the PDZ domain of PSD-95, also has a PDZ-binding motif at its C-terminal end, -ESDV; however, the C-terminal segment of NR2B did not bind to myc-mShank3/SH3-PDZ (Fig. 3b). These findings demonstrate that the final four aa of GluR1 subunit are important for specific binding to the PDZ domain of mShank3.

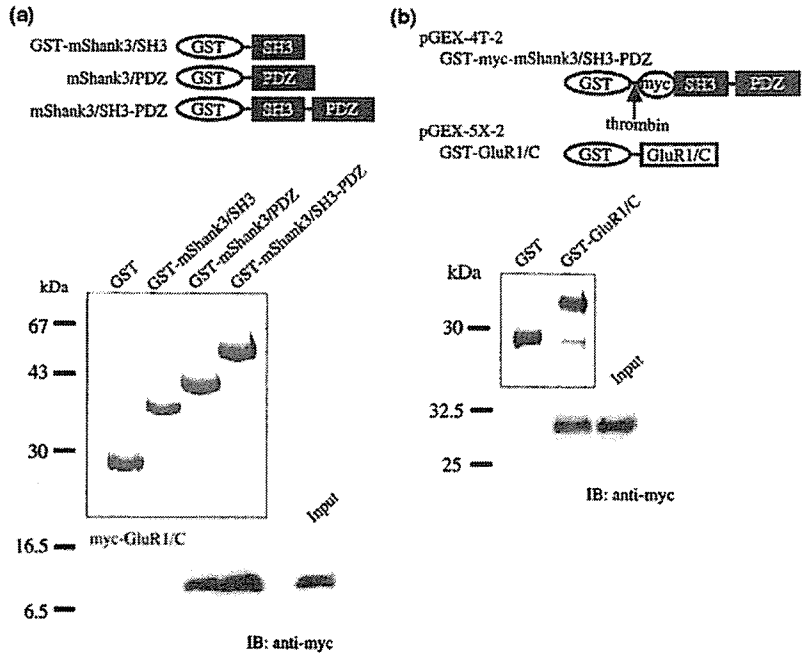

Fig. 2 Direct interaction of mouse Shank3 (mShank3) with GluR1 subunit. (a) Pull-down assay. The schematic structure of glutathione S-transferase (GST)-fused mShank3 mutants is shown at the top. The upper panel shows the purified GST and GST-fused mShank3 proteins separated by sodium dodecyl sulfate–polyacrylamide gel electrophoresis (SDS–PAGE) and the lower panels show the immunoblot. GST alone or each of the GST-fusion proteins bound to glutathione sepharose beads was incubated with 400 μg of extract from Chinese hamster ovary (CHO) cells transfected with myc-tagged GluR1/C. After washing, the proteins on the beads were eluted with SDS–PAGE sample buffer and immunoblotted with anti-myc antibody. The input lane was loaded with 30 μg of the CHO cells extract. (b) Pull-down assay. The schematic structure of GST-fused mShank3/SH3-PDZ and GluR1/C is shown at the top. The upper panel shows the purified GST and GST-fused GluR1/C proteins separated by SDS–PAGE and the lower panels show the immunoblots. GST alone or GST-fused GluR1/C bound to glutathione sepharose beads was incubated with purified myc-Shank3/SH3-PDZ. After washing, the proteins on the beads were eluted with SDS–PAGE sample buffer and immunoblotted with anti-myc antibody. The input lane was loaded with 5% of the purified myc-Shank/SH3-PDZ used for the pull-down assay. Molecular weight standards are shown on the left. PDZ, post-synaptic density-95/Dlg/ZO-1; SH3, Src homology 3; IB, immunoblot.

We then investigated the interaction between mShank3 and full-length GluR1 subunit by immunoprecipitation experiments. We constructed myc-tagged mShank3 (myc-mShank3) and the four deletion mutants as shown in Fig. 4(a), and expressed them together with EGFP-GluR1 in COS7 cells. Anti-EGFP antibody coimmunoprecipitated myc-mShank3, myc-mShank3/PDZ + C, myc-mShank3/SH3-PDZ and myc-mShank3/PDZ from cell lysates of COS7 cells expressing EGFP-GluR1 and myc-mShank3 or deletion mutants but not myc-mShank3/C (Fig. 4b). No signals were observed with immunoprecipitates obtained with normal IgG. These results indicate that the PDZ domain of mShank3 is indispensable to the interaction with GluR1 subunit.

Mouse Shank3 is expressed in the spine of the cortical neurons and interacts with GluR1 α-amino-3-hydroxy-5-methyl-4-isoxazole propionic acid receptor

To study native mShank3 protein, rabbit polyclonal antibodies were raised against the GST-fused 342-aa segment of mShank3 (aa 1016–1357). To confirm the specificity of the anti-mShank3 antibody, we transiently transfected COS cells with myc-mShank3 to allow the use of anti-myc antibody as a positive control. As shown in Fig. 5(a), the immunoreactive band for anti-mShank3 antibody (240 kDa) was identical to that for anti-myc antibody and no bands were detected in the COS7 cells transfected with myc vector, indicating that the anti-mShank3 antibody specifically detected mShank3 protein. mShank3-immunoreactive bands were observed in mouse cortical lysates and disappeared upon coincubation with antigen GST-fused mShank3 segment but not with GST alone (data not shown). We also confirmed the presence of mShank3 in the synaptosomal fraction as well as GluR1 subunit and PSD-95 (Fig. 5b).

To verify the interaction between mShank3 and GluR1 AMPA receptor *in vivo*, we performed a coimmunoprecipitation assay with membrane fraction prepared from mouse cortex using anti-Shank3 antibody (Fig. 5c). Shank3 antibody efficiently immunoprecipitated endogenous mShank3

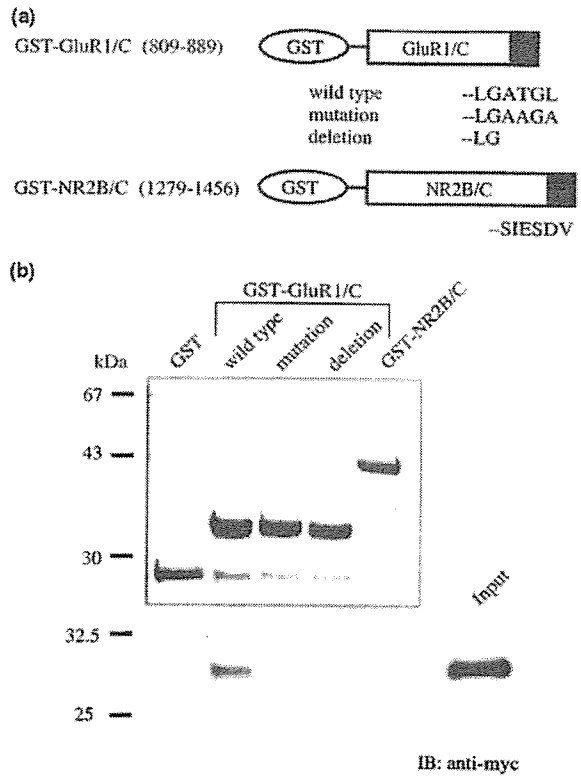

Fig. 3 Role of the post-synaptic density-95/Dlg/ZO-1 (PDZ) binding motif of GluR1 in the interaction with mouse Shank3 (mShank3)/SH3-PDZ. (a) The schematic description of glutathione S-transferase (GST)-fused GluR1/C and C-terminal segment of NMDA receptor 2B (NR2B/C) proteins. (b) Pull-down assay. The upper panel shows the purified GST and GST-fused proteins separated by sodium dodecyl sulfate–polyacrylamide gel electrophoresis (SDS–PAGE) and the lower panel shows the immunoblots. GST alone or each of the GST-fusion proteins bound to glutathione sepharose beads was incubated with 200 μg of extract from Chinese hamster ovary (CHO) cells transfected with myc-tagged mShank3/SH3-PDZ. After washing, the proteins on the beads were eluted with SDS–PAGE sample buffer and immunoblotted with anti-myc antibody. The input lane was loaded with 10 μg of the CHO cells extract. Molecular weight standards are shown on the left. SH3, Src homology 3; IB, immunoblot.

protein and coprecipitated GluR1 subunit, while normal IgG immunoprecipitated neither mShank3 nor GluR1 subunit. This finding suggests that mShank3 interacts with GluR1 AMPA receptor in mouse cortex.

We next used this antibody to examine cortical primary neurons for expression of mShank3 and the pattern of mShank3 immunoreactivity was found to be strikingly punctate. To clarify the distribution of mShank3, EGFP was transfected into neurons and its signal was superimposed on the mShank3 staining. As shown in Fig. 5(d), judging from their morphology mShank3 was mainly expressed in the spines. Moreover, the punctate signals of mShank3 closely coincided with those of PSD-95 (Fig. 5e), indicating that mShank3 was colocalized with PSD-95 in the spines.

Mouse Shank3 interacts with membrane-surface GluR1 subunit in the spines

As the GST pull-down and immunoprecipitation experiments demonstrated the biochemical interaction of mShank3 with GluR1 subunit, we investigated the interaction of these proteins in neurons. We constructed a plasmid, EGFP-GluR1, in which EGFP had been fused with the extracellular region of GluR1, and transfected it into cortical neurons cultured for 12 days. When we examined them 2 days later, the EGFP fluorescence perfectly matched the GluR1 staining (data not shown). Under permeant conditions, in which proteins located on both the intracellular and membrane surface are detected, immunostaining with anti-EGFP antibody revealed expression of EGFP-GluR1 in the cell body, neuritis and spines (Fig. 5f, i). By contrast, the EGFP-GluR1 staining was punctate when the anti-EGFP antibody was applied to a living culture under non-permeant conditions to detect EGFP-GluR1 delivered onto the membrane surface (Fig. 5f, ii), indicating that the membrane-surface EGFP-GluR1 forms clusters. Subsequent staining of the same neurons for PSD-95 under permeant conditions showed that the punctate EGFP-GluR1 staining coincided with the PSD-95 staining (Fig. 5f, iii), implying that the membrane-surface EGFP-GluR1 was distributed in the spines. This finding is consistent with previous reports that almost all membrane-surface GluR1 clusters are synaptic (Shi *et al.* 1999). At 2 days after cotransfection with myc-mShank3 and EGFP-GluR1, EGFP-GluR1 staining was performed with anti-EGFP antibody under non-permeant conditions and followed by myc-mShank3 staining with anti-myc antibody under permeant conditions. Many punctate myc-mShank3 staining signals were colocalized with those of EGFP-GluR1 staining (EGFP-GluR1/myc-mShank3 colocalization rate 80.0 ± 3.8%; $n = 5$) (Fig. 5g). At 1 week after cotransfection, the mShank3 staining was as strikingly punctate as native mShank3 staining and merged well with the EGFP-GluR1 staining in the spines (Fig. 5h). These results suggest that mShank3 interacts with membrane-surface GluR1 subunit.

All members of the mouse Shank family are expressed in the cortex and may interact with GluR1 subunit

Previous studies have shown that all three members of the Shank family are expressed in rat cortex. We investigated the expression and distribution of Shank mRNAs in the mouse cortex by *in situ* hybridization during post-natal development on post-natal days 1 and 15 and at 8 weeks of age. Antisense cRNA probes transcribed from each mShank gene specifically recognized particular mShank transcripts whereas sense cRNA probes did not (data not shown). As shown in Fig. 6(a), the hybridization signals for mShank1 and mShank2 mRNAs were detected at all post-natal stages

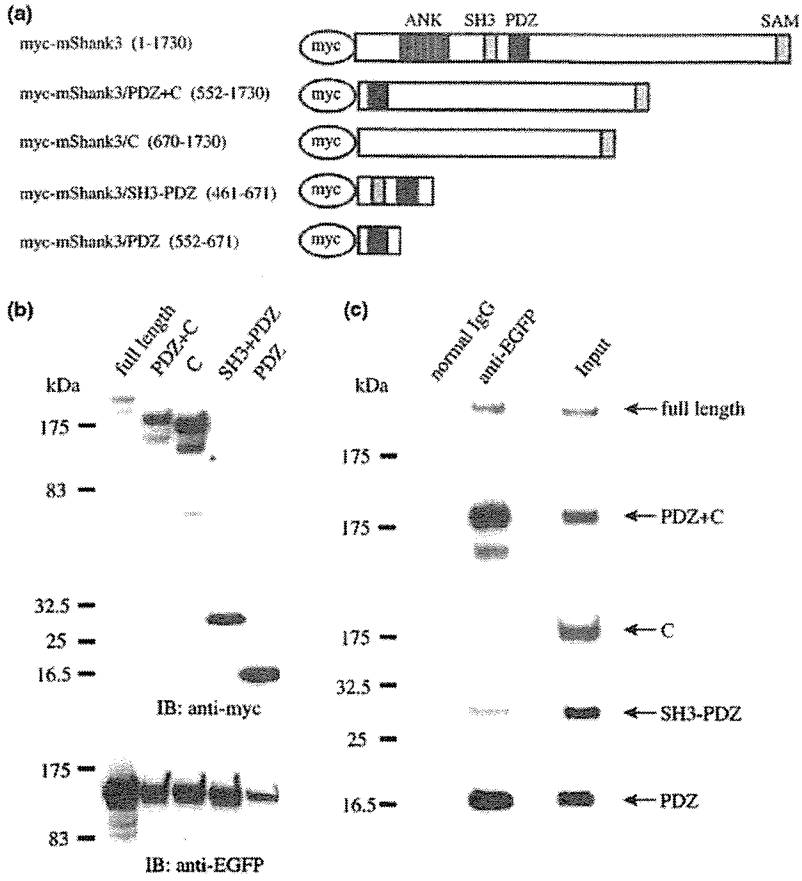

Fig. 4 GluR1 binds to the post-synaptic density-95/Dlg/ZO-1 (PDZ) domain of mouse Shank3 (mShank3). (a) Schematic structure of myc-tagged mShank3 mutants. (b) Immunoblot analysis. COS7 cells were transfected with each of the myc-tagged mShank3 mutants together with enhanced green fluorescent protein-fused GluR1 subunit (EGFP-GluR1). Lysates of transfected COS7 cells (5 μg of proteins) were separated by sodium dodecyl sulfate–polyacrylamide gel electrophoresis (SDS–PAGE) and immunoblotted with anti-myc antibody (upper panel) and with anti-enhanced green fluorescent protein (EGFP) antibody (lower panel). (c) Immunoprecipitation assay. Normal rabbit IgG or anti-EGFP antibody bound to Protein A- and G-Sepharose beads was incubated with 300 μg of extract from COS7 cells cotransfected with EGFP-GluR1 and myc-tagged mShank3 mutant. After washing, the proteins on the beads were eluted with SDS–PAGE sample buffer and immunoblotted with anti-myc antibody. Molecular weight standards are shown on the left. ANK, Ankyrin repeats 1–7; SH3, Src homology 3 domain; SAM, sterile alpha motif; IB, immunoblot.

measured; however, expression of mShank3 mRNA was clearly seen at post-natal days 1 and 15 and the signals at 8 weeks of age were very faint. These results were confirmed by RT-PCT (Fig. 6b) and immunoblot analysis (Fig. 6c). On the other hand, the distribution of the mRNAs of all members of the Shank family in the cortex was not significantly different. Thus, it appears that mShank1, mShank2 and mShank3 are expressed in the same neurons in cortex. Finally, we investigated whether mShank1 and mShank2 interact with GluR1 subunit, because the SH3-PDZ domain is well conserved among all members of the Shank family. As shown in Fig. 6(d), mShank1/SH3-PDZ and mShank2/SH3-PDZ also bound GluR1/C, the same as mShank3/SH3-PDZ.

Discussion

In this study we used a yeast two-hybrid screening system and identified a synaptic molecule that interacts with GluR1 subunit of AMPA receptors. The molecule, named Shank3/ProSAP2, is a multidomain protein localized in PSDs which links cell-surface receptors, including various types of GluRs, to the actin-based cytoskeleton (Lim *et al.* 1999; Naisbitt *et al.* 1999; Sheng and Kim 2000; Böckers *et al.* 2001, 2002). The most striking finding in our study was that GluR1 subunit is capable of directly binding to the PDZ domain of the Shank3 via its C-terminal PDZ-binding motif (four aa sequence, -ATGL), while GluR2 subunit indirectly binds to the SH3 domain of the Shank protein mediated by glutamate receptor-interacting protein (GRIP) (Sheng and Kim 2000). The PDZ domain is a stretch of 80–100 aa residues which plays an important role in protein–protein interaction (Songyang *et al.* 1997). Thus far it has been reported that synaptic proteins containing a type I PDZ-binding motif (the C-terminal four-amino-acid sequence -X-T/S-X-V/L/I, where X represents any aa), such as GKAP/SAP90/PSD-95-associated protein (SAPAP) (-QTRL), the somatostatin receptor 2 (-QTSI) and the calcium-independent α-latrotoxin receptor (-VTSL), bind to the PDZ domain of Shank (Böckers *et al.* 2002) and thus, the PDZ domain of Shank is thought to be a type I PDZ. As expected, no binding of the GluR2 subunit of AMPA receptors was observed in our study, as GluR2 subunit possesses a type II, not type I, PDZ-binding motif. Interestingly, however, little or no binding of the NR2B subunit was observed, even though NR2B subunit has a type I PDZ-binding motif

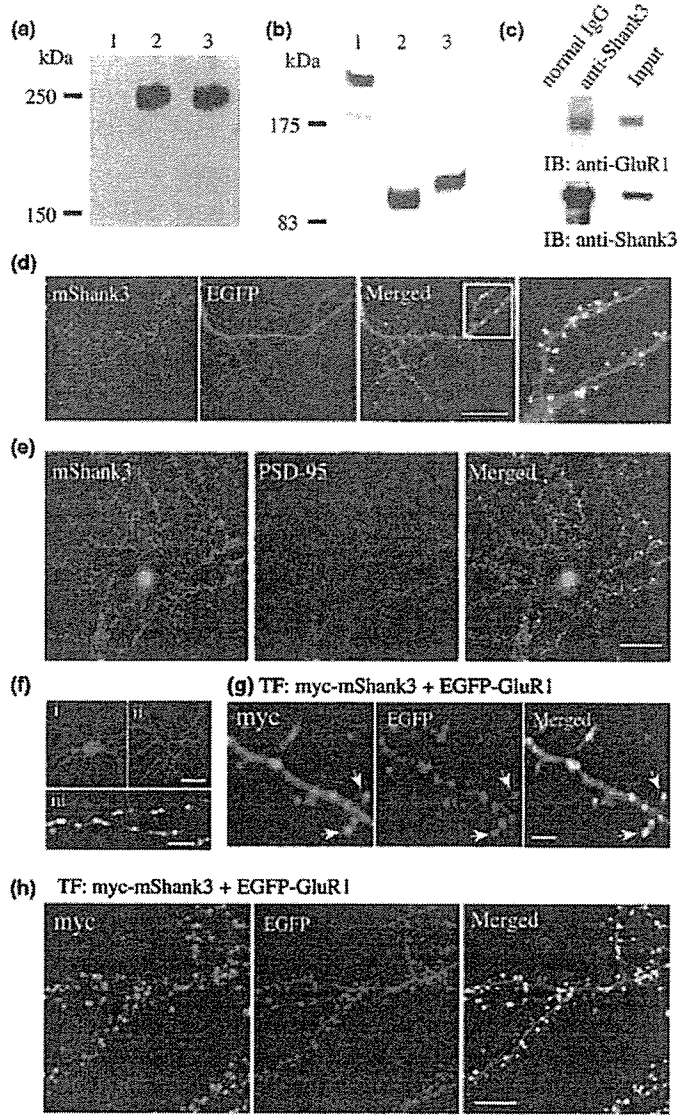

Fig. 5 Expression and distribution of mouse Shank3 (mShank3) in cortical neurons. (a) Immunoblot analysis. Lysates of COS7 cells (5 μg of proteins) transfected with myc (lane 1) or myc-mShank3 (lanes 2 and 3) were separated by sodium dodecyl sulfate–polyacrylamide gel electrophoresis (SDS–PAGE) and immunoblotted with anti-mShank3 antibody (lanes 1 and 2) and with anti-myc antibody (lane 3). (b) Immunoblot analysis. Synaptosomal proteins (30 μg) were separated by SDS–PAGE and immunoblotted with anti-mShank3 antibody (lane 1), anti-post-synaptic density-95 (PSD-95) antibody (lane 2) or anti-GluR1 antibody (lane 3). Molecular weight standards are shown on the left. (c) Immunoprecipitation assay. Normal rabbit IgG or anti-Shank3 antibody bound to Protein A- and G-Sepharose beads was incubated with 1 mg of membrane fraction from mouse cortex. After washing, the proteins on the beads were eluted with SDS–PAGE sample buffer and immunoblotted with anti-GluR1 antibody. The input lane was loaded with 50 μg of membrane fraction. (d) Cortical neurons cultured for 12 days were transfected with enhanced green fluorescent protein (EGFP). At 2 days later, the neurons were fixed and stained with anti-mShank3 antibody. An enlargement of the square field indicated is shown in the right panel. (e) Cortical neurons were cultured for 18 days and double-stained with anti-mShank3 antibody (red) and anti-PSD-95 antibody (green). (f) Cortical neurons cultured for 12 days were transfected with EGFP-fused GluR1 subunit (EGFP-GluR1). After 2 days, the neurons were stained with anti-EGFP antibody under permeant (i) or non-permeant (ii) conditions. The immunoreactive signals for anti-EGFP antibody (green) under non-permeant conditions were matched with those for anti-PSD-95 antibody (red) (iii). (g) Cortical neurons cultured for 12 days were transfected with myc-mShank3 and EGFP-GluR1. At 2 days later, the neurons were stained with anti-EGFP antibody (green) under non-permeant conditions and with anti-myc antibody (red) after fixation. The arrows point to examples of overlapping signals. (h) Cortical neurons cultured for 12 days were transfected with myc-mShank3 and EGFP-GluR1. At 7 days later, the neurons were stained with anti-EGFP antibody (green) and anti-myc antibody (red). Scale bars: 30 μm (d) and 15 μm (e, panels i and ii in f), 10 μm (h) and 5 μm (panel iii in f and g). IB, immunoblot; TF, transfection.

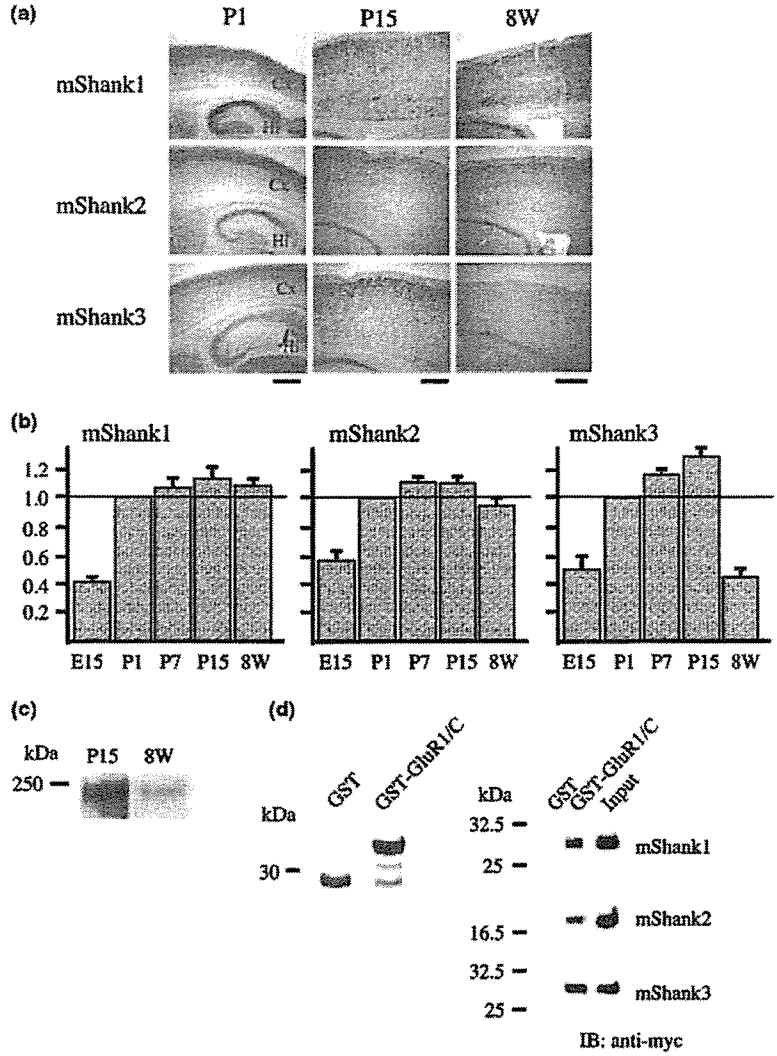

Fig. 6 Expression of mouse Shank (mShank) mRNAs in developing mouse cortex and interaction of mShank proteins with GluR1 subunit. (a) *In situ* hybridization analysis. Distribution of mShank mRNAs in the post-natal mouse cortex. Cx, cortex; Hi, hippocampus. Scale bar, 500 μm. (b) RT-PCR analysis. Amounts of total RNA used for the PCR were normalized to glyceraldehyde-3-phosphate dehydrogenase. The relative strength of the band signals was measured with NIH Imaging software and the ratio was calculated by dividing the value at each stage by the value at post-natal day (P)1. (c) Immunoblot analysis. Lysates of cortex (30 μg) prepared from P15 or 8-week-old mice were separated by sodium dodecyl sulfate–polyacrylamide gel electrophoresis (SDS–PAGE) and immunoblotted with anti-mShank3 antibody. (d) Pull-down assay. The left panel shows the purified glutathione S-transferase (GST) and GST-fused GluR1/C separated by SDS–PAGE and the right panels show the immunoblots. GST alone or GST-fused GluR1/C bound to glutathione sepharose beads was incubated with 300 μg of extract from Chinese hamster ovary (CHO) cells transfected with myc-tagged mShank/SH3-PDZ. After washing, the proteins on the beads were eluted with SDS–PAGE sample buffer and immunoblotted with anti-myc antibody. The input lane was loaded with 10 μg of the CHO cell extract. Molecular weight standards are shown on the left. PDZ, post-synaptic density-95/Dlg/ZO-1; SH3, Src homology 3 domain; 8W, 8 weeks of age; IB, immunoblot.

(-ESDV) by which NR2B subunit binds to the type I PDZ domain of PSD-95. The above findings suggest that the binding partners of Shank via the PDZ domain are highly selective molecules. A recent analysis of the crystal structure of the PDZ domain of the Shank–peptide ligand (EAQTRL) complex has revealed that the carboxylate binding loop formed by the second β-strand within the PDZ domain is critical for binding to the peptide ligand (Im *et al.* 2003). The aa sequence of the second β-strand is identical in all three members of the Shank family. The recent structural studies support our result showing that GluR1/C not only bound to Shank3 but also to Shank1 and Shank2.

The biochemical interaction of mShank3 with GluR1 subunit was complemented by coimmunoprecipitation assay with membrane fraction prepared from mouse cortex using anti-Shank3 antibody and by transfection experiments showing colocalization of Shank3 with GluR1 subunit in the spines of mouse cultured cortical neurons. When myc-mShank3 was expressed with EGFP-GluR1 in maturing cortical neurons, many myc-mShank3 clusters colocalized with cell-surface EGFP-GluR1. Shi *et al.* (1999) reported that cell-surface recombinant EGFP-GluR1, the same construct as our plasmid, expressed in hippocampal neurons displayed a punctate distribution that colocalized with both surface labeling of endogenous GluR2 subunit and with a pre-synaptic marker, synapsin. Therefore, our results suggest that myc-mShank3 colocalizes with functional AMPA receptors containing GluR1 subunit at synaptic sites.

Recent cumulative evidence has shown that the clustering of AMPA receptors at the post-synaptic membrane is critical for synaptic maturation and plasticity. As trafficking of GluR1 subunit to synapses was diminished by mutating the PDZ interacting region of GluR1 subunit, the trafficking may be mediated by a family of PDZ-domain-containing proteins (Hayashi *et al.* 2000; Shi *et al.* 2001). However, the binding partner of GluR1 subunit remains to be determined. One candidate is SAP-97, a type I PDZ protein homologous to PSD-95, and the biochemical interaction of SAP-97 with GluR1 subunit has actually been demonstrated (Leonard *et al.* 1998). During development, however, expression of SAP-97 is distributed more in the somatic region than in the dendrites, although it is found along dendrites, presumably at synaptic sites, in mature neurons (Valtschanoff *et al.* 2000). Thus, SAP-97 is thought to be associated with intracellular AMPA receptors, including GluR1 subunit, and to be involved in the early secretory pathway, endoplasmic reticulum/cis-Golgi pathway, of AMPA receptors trafficking during development (Sans *et al.* 2001). Shank3, on the other hand, is expressed in post-synaptic sites where the functional AMPA receptors are localized. Roussignol *et al.* (2005) recently showed that transfection of Shank3 into cerebellar granule cells increased the AMPA component of mEPSCs. Thus, Shank3 is an intriguing molecule that interacts with AMPA receptors and regulates their function at post-synaptic sites. The mechanism of activity-depending AMPA receptor trafficking to synapses involving Shank3 needs to be more thoroughly elucidated.

In situ hybridization and RT-PCR analyses have shown that Shank3 mRNA expression in mouse cortex increases after birth and gradually decreases during later development, consistent with previous studies on rat brain (Böckers *et al.* 2001, 2004). Thus, Shank3 may play an important role in neural functions, such as synaptogenesis and synapse maturation, at an early stage of post-natal development rather in adulthood. However, Shank1 and Shank2 mRNAs are also expressed in cortical neurons after birth and their expression levels are sustained into adulthood. Furthermore, the expression patterns of all three Shank mRNAs in the cortex do not significantly differ. The members of the Shank family share essentially the same domain structures, such as the SH3 and PDZ domains, and lower homologous regions, such as the proline-rich region. Thus, it has been thought that the individual members of the Shank family may have unique functions in addition to their common function as scaffold proteins but little is known about their other functions. Further study, especially in Shank knock-out and transgenic mouse, should provide useful insights into the functions of the individual members of the Shank family in regard to synaptogenesis, synapse maturation and subsequent formation of neural networks. Interestingly, recent genetic analyses of the 22q13.3 deletion syndrome, which is characterized by global developmental delay, absent or severely delayed speech and hypotonia, have suggested that the haplo-insufficiency for Shank3 is probably the cause of the pathological state as the Shank3 gene is located on chromosome 22q13.3 (Bonaglia *et al.* 2001; Wilson *et al.* 2003). Thus, clinical studies may lead to elucidation of the particular function of Shank3 and clarification of the specific function of Shank3 may lead to novel strategies for the treatment of this syndrome.

Acknowledgements

We thank Dr Masayoshi Mishina for the GluR1 (GluRα1), GluR2 (GluRα2) and NR2B (GluRε2) cDNAs. This study was supported by a grant from the Ministry of Health, Labour and Welfare, Japan.

References

Bliss T. V. P. and Collingridge G. L. (1993) A synaptic model of memory: long-term potentiation in the hippocampus. *Nature* **361**, 31–39.

Böckers T. M., Mameza M. G., Kreutz M. R., Bockmann J., Weise C., Buck F., Richter D., Gundelfinger E. D. and Kreienkamp H.-J. (2001) Synaptic scaffolding proteins in rat brain. Ankyrin repeats of the multidomain Shank protein family interact with the cytoskeletal protein α-fodrin. *J. Biol. Chem.* **276**, 40 104–40 112.

Böckers T. M., Bockmann J., Kreutz M. R. and Gundelfinger E. D. (2002) ProSAP/Shank proteins – a family of higher order organizing molecules of the postsynaptic density with an emerging role in human neurological disease. *J. Neurochem.* **81**, 903–910.

Böckers T. M., Segger-Junius M., Iglauer P., Bockmann J., Gundelfinger E. D., Kreutz M. R., Richter D., Kindler S. and Kreienkamp H.-J. (2004) Differential expression and dendritic transcript localization of Shank family members: identification of a dendritic targeting element in the 3′ untranslated region of Shank1 mRNA. *Mol. Cell Neurosci.* **26**, 182–190.

Bonaglia M. C., Giorda R., Borgatti R., Felisari G., Gagliardi C., Selicorni A. and Zuffardi O. (2001) Disruption of the ProSAP2 gene in a t(12;22)(q24.1;q13.3) is associated with the 22q13.3 deletion syndrome. *Am. J. Hum. Genet.* **69**, 261–268.

Carlin R. K., Grab D. J., Cohen R. S. and Siekevitz P. (1980) Isolation and characterization of postsynaptic densities from various brain regions: enrichment of different types of postsynaptic densities. *J. Cell Biol.* **86**, 831–843.

Chomczynski P. and Sacchi N. (1987) Single-step method of RNA isolation by acid guanidinium thiocyanate-phenol-chloroform extraction. *Anal. Biochem.* **162**, 156–159.

Cohen N. A., Brenman J. E., Snyder S. H. and Bredt D. S. (1996) Binding of the inward rectifier K^+ channel Kir 2.3 to PSD-95 is regulated by protein kinase A phosphorylation. *Neuron* **17**, 759–767.

Durand G. M., Kovalchuk Y. and Konnerth A. (1996) Long-term potentiation and functional synapse induction in developing hippocampus. *Nature* **381**, 71–75.

Hayashi Y., Shi S.-H., Esteban J. A., Piccini A., Poncer J.-C. and Malinow R. (2000) Driving AMPA receptors into synapses by LTP and CaMKII: Requirement for GluR1 and PDZ domain interaction. *Science* **287**, 2262–2267.

Hirasawa T., Wada H., Kohsaka S. and Uchino S. (2003) Inhibition of NMDA receptors induces delayed neuronal maturation and sustained proliferation of progenitor cells during neocortical development. *J. Neurosci. Res.* **74**, 676–687.

Hollmann M. and Heinemann S. (1994) Cloned glutamate receptors. *Annu. Rev. Neurosci.* **17**, 31–108.

Im Y. J., Lee J. H., Park S. H., Park S. J., Rho S.-H., Kang G. B., Kim E. and Eom S. H. (2003) Crystal structure of the Shank PDZ-ligand complex reveals a class I PDZ interaction and a novel PDZ-PDZ dimerization. *J. Biol. Chem.* **278**, 48 099–48 104.

Isaac J. T. (2003) Postsynaptic silent synapses: evidence and mechanisms. *Neuropharmacology* **45**, 450–460.

Leonard A. S., Davare M. A., Horne M. C., Garner C. C. and Hell J. W. (1998) SAP97 is associated with the α-amino-3-hydroxy-5-methylisoxazole-4-propionic acid receptor GluR1 subunit. *J. Biol. Chem.* **273**, 19 518–19 524.

Liao D., Scannevin R. H. and Huganir R. (2001) Activation of silent synapses by rapid activity-dependent synaptic recruitment of AMPA receptors. *J. Neurosci.* **21**, 6008–60017.

Lim S., Naisbitt S., Yoon J., Hwang J.-I., Suh P.-G., Sheng M. and Kim E. (1999) Characterization of the shank family of synaptic proteins. Multiple genes, alternative splicing, and differential expression in brain and development. *J. Biol. Chem.* **274**, 29 510–29 518.

McDonald J. W. and Johnston M. V. (1990) Physiological and pathophysiological roles of excitatory amino acids during central nervous system development. *Brain Res. Brain Res. Rev.* **15**, 41–70.

Naisbitt S., Kim E., Tu J. C., Xiao B., Sala C., Valtschanoff J., Weinberg R. J., Worley P. F. and Sheng M. (1999) Shank, a novel family of postsynaptic density proteins that binds to the NMDA receptor/PSD-95/GKAP complex and cortactin. *Neuron* **23**, 569–582.

Pickard L., Noël J., Henley J. M., Collingridge G. L. and Molnar E. (2000) Developmental changes in synaptic AMPA and NMDA receptor distribution and AMPA receptor subunit composition in living hippocampal neurons. *J. Neurosci.* **20**, 7922–7931.

Roussignol G., Ango F., Romorini S., Tu J. C., Sala C., Worley P. F., Bockaert J. and Fagni L. (2005) Shank expression is sufficient to induce functional dendritic spine synapses in aspiny neurons. *J. Neurosci.* **25**, 3560–3570.

Sans N., Racca C., Petralia R. S., Wang Y.-X., McCallum J. and Wenthold R. J. (2001) Synapse-associated protein 97 selectively associates with a subset of AMPA receptors early in their biosynthetic pathway. *J. Neurosci.* **21**, 7506–7516.

Sheng M. and Kim E. (2000) The Shank family of scaffold proteins. *J. Cell Sci.* **113**, 1851–1856.

Shi S.-H., Hayashi Y., Petralia R. S., Zaman S. H., Wenthold R. J., Svoboda K. and Malinow R. (1999) Rapid spine delivery and redistribution of AMPA receptors after synaptic NMDA receptor activation. *Science* **284**, 1811–1816.

Shi S.-H., Hayashi Y., Esteban J. A. and Malinow R. (2001) Subunit-specific rules governing AMPA receptor trafficking to synapses in hippocampal pyramidal neurons. *Cell* **105**, 331–343.

Songyang Z., Fanning A. S., Fu C., Xu J., Marfatia S. M., Chishti A. H., Crompton A., Chan A. C., Anderson J. M. and Cantley L. C. (1997) Recognition of unique carboxyl-terminal motifs by distinct PDZ domains. *Science* **275**, 73–77.

Tu J. C., Xiao B., Naisbitt S. *et al.* (1999) Coupling of mGluR/Homer and PSD-95 complexes by the Shank family of postsynaptic density proteins. *Neuron* **23**, 583–592.

Valtschanoff J. G., Burette A., Davare M. A., Leonard A. S., Hell J. W. and Weinberg R. J. (2000) SAP97 concentrates at the postsynaptic density in cerebral cortex. *Eur. J. Neurosci.* **12**, 3605–3614.

Wilson H. L., Wong A. C., Shaw S. R., Tse W. Y., Stapleton G. A., Phelan M. C., Hu S., Marshall J. and McDermid H. E. (2003) Molecular characterization of the 22q13.3 deletion syndrome supports the role of haploinsufficiency of SHANK3/PROSAP2 in the major neurological symptoms. *J. Med. Genet.* **40**, 575–584.

Wisden W. and Seeburg P. H. (1993) Mammalian ionotropic glutamate receptors. *Curr. Opin. Neurobiol.* **3**, 291–298.

Wu G., Malinow R. and Cline H. T. (1996) Maturation of a central glutamatergic synapse. *Science* **274**, 972–976.

Zhu J. J., Esteban J. A., Hayashi Y. and Malinow R. (2000) Postnatal synaptic potentiation: delivery of GluR4-containing AMPA receptors by spontaneous activity. *Nat. Neurosci.* **3**, 1098–1106.

GLIA 55:604–616 (2007)

Involvement of $P2X_4$ and $P2Y_{12}$ Receptors in ATP-Induced Microglial Chemotaxis

KEIKO OHSAWA,[1] YASUHIRO IRINO,[1] YASUKO NAKAMURA,[1] CHIHIRO AKAZAWA,[1] KAZUHIDE INOUE,[2] AND SHINICHI KOHSAKA[1]*

[1]*Department of Neurochemistry, National Institute of Neuroscience, Kodaira, Tokyo 187-8502, Japan*

[2]*Department of Pharmacology, Graduate School of Pharmaceutical Sciences, Kyushu University, Higashi, Fukuoka 812-8582, Japan*

KEY WORDS

microglia; ATP; chemotaxis; P2Y12; P2X4

ABSTRACT

We previously reported that extracellular ATP induces membrane ruffling and chemotaxis of microglia and suggested that their induction is mediated by the Gi/o-protein coupled $P2Y_{12}$ receptor ($P2Y_{12}R$). Here we report discovering that the $P2X_4$ receptor ($P2X_4R$) is also involved in ATP-induced microglial chemotaxis. To understand the intracellular signaling pathway downstream of $P2Y_{12}R$ that underlies microglial chemotaxis, we examined the effect of two phosphatidylinositol 3′-kinase (PI3K) inhibitors, wortmannin, and LY294002, on chemotaxis in a Dunn chemotaxis chamber. The PI3K inhibitors significantly suppressed chemotaxis without affecting ATP-induced membrane ruffling. ATP stimulation increased Akt phosphorylation in the microglia, and the increase was reduced by the PI3K inhibitors and a $P2Y_{12}R$ antagonist. These results indicate that $P2Y_{12}R$-mediated activation of the PI3K pathway is required for microglial chemotaxis in response to ATP. We also found that the Akt phosphorylation was reduced when extracellular calcium was chelated, suggesting that ionotropic P2X receptors are involved in microglial chemotaxis by affecting the PI3K pathway. We therefore tested the effect of various $P2X_4R$ antagonists on the chemotaxis, and the results showed that pharmacological blockade of $P2X_4R$ significantly inhibited it. Knockdown of the $P2X_4$ receptor in microglia by RNA interference through the lentivirus vector system also suppressed the microglial chemotaxis. These results indicate that $P2X_4R$ as well as $P2Y_{12}R$ is involved in ATP-induced microglial chemotaxis.

INTRODUCTION

Microglia are the immune effector cells that participate in tissue repair, amplification of inflammatory responses, and neuronal degeneration in the central nervous system (CNS) (Kreutzberg, 1996; Streit, 2002). They are present in the form of ramified cells under normal conditions, but in response to pathological stimuli microglia rapidly transform into a motile ameboid form and migrate toward lesion sites, where they secrete a variety of substances and clear cell debris (Moran and Graeber, 2004; Nakajima and Kohsaka, 2005; Stence et al., 2001). Thus, microglial migration plays a crucial role in the amelioration of a damaged CNS; however, the intracellular signals underlying microglial cell migration are poorly understood.

Extracellular ATP is known to play a role as a neurotransmitter or neuromodulator in the CNS (Illes and Alexandre Ribeiro, 2004), and it regulates various physiological functions of microglia (Inoue, 2002). ATP receptors are classified into two families: the ionotropic P2X receptor (P2XR) family and the GTP-binding (G-) protein coupled P2Y receptor (P2YR) family (Ralevic and Burnstock, 1998), and microglia have been reported to possess functional ATP receptors, including $P2X_4R$, $P2X_7R$, and $P2Y_{12}R$ (Cavaliere et al., 2003; James and Butt, 2002; Sasaki et al., 2003; Tsuda et al., 2003). Davalos et al. (2005) and Nimmerjahn et al. (2005) recently reported that processes of ramified microglia extended toward a confocal laser injury, where ATP is likely to be released by damaged tissue and surrounding astrocytes. These observations suggest that ATP is a primary molecule in the induction of the change in microglial morphology.

We have also previously reported that ATP-induced microglial membrane ruffling and chemotaxis are mediated by Gi/o-protein coupled $P2Y_{12}R$ (Honda et al., 2001; Sasaki et al., 2003); however, the intracellular signaling pathway downstream of $P2Y_{12}R$ following ATP stimulation is not fully understood. Several recent articles have revealed that $P2Y_{12}R$ stimulation results in activation of the phosphatidylinositol 3′-kinase (PI3K) pathway in some cells (Czajkowski et al., 2004; Soulet et al., 2004; Van Kolen and Slegers, 2004). Although PI3K is known to be a crucial enzyme in the regulation of chemotaxis by monocytes and macrophages (Procko and McColl, 2005; Ridley, 2001; Van Haastert and Devreotes, 2004), whether the PI3K pathway participates in ATP-induced microglial chemotaxis remained unclear.

This article contains supplementary material available via the Internet at http://www.interscience.wiley.com/jpages/0894-1491/suppmat

Grant sponsors: Japanese Ministry of Health, Labour, and Welfare; Japanese Ministry of Education, Culture, Sports, Science, and Technology.

*Correspondence to: Shinichi Kohsaka, Department of Neurochemistry, National Institute of Neuroscience, 4-1-1 Ogawahigashi, Kodaira, Tokyo 187-8502, Japan. E-mail: kohsaka@ncnp.go.jp

Received 7 August 2006; Accepted 26 December 2006

DOI 10.1002/glia.20489

Published online 13 February 2007 in Wiley InterScience (www.interscience.wiley.com).

In this study we demonstrated that activation of the PI3K pathway is required for ATP-induced microglial chemotaxis and found that the PI3K/Akt activation was suppressed when extracellular Ca^{2+} was chelated. ATP stimulates P2XRs in microglia and causes an increase in intracellular calcium concentration ($[Ca^{2+}]_i$) by inducing an extracellular Ca^{2+} influx (Inoue et al., 1998; Tsuda et al., 2003). Therefore, to clarify involvement of P2XRs in microglial chemotaxis we also examined the effect of antagonists and RNA interference (RNAi) with P2XRs on microglial chemotaxis, and the results demonstrated that P2X$_4$R is involved in ATP-induced chemotaxis.

MATERIALS AND METHODS

Isolation of Microglia

Microglia were obtained from primary cell cultures of neonatal Wistar rat cerebral cortex as described previously (Nakajima et al., 1992). In brief, mixed glial cultures were maintained for 12–23 days in DMEM (Invitrogen, Carlsbad, CA) with 10% fetal calf serum (FCS) (Irvine Scientific, Santa Ana, CA). Microglia were prepared as floating cells by gentle shaking and allowed to attach to appropriate dishes or glasses.

Membrane Ruffling

Microglia attached to glass coverslips were incubated for 4 h in DMEM without FCS and stimulated with 50 μM ATP (Yamasashyoyu, Chiba, Japan) for 5 min at 37°C. The cells were then fixed with 3.7% formaldehyde for 10 min, permeabilized for 5 min with PBS containing 0.1% Triton X-100, and stained for 1 h with 2 U/mL Texas Red-conjugated phalloidin (Invitrogen) diluted in PBS containing 1%BSA. The cells were mounted in PermaFluor (Thermo Fisher Scientific, Waltham, MA) and examined under a fluorescence microscope AX70 (Olympus, Tokyo, Japan). To quantify membrane ruffles, cells were stained with 1 μg/mL anti-Iba1 polyclonal antibody (Imai et al., 1996) and Alexa Fluor 488-conjugated anti-rabbit IgG (1:1,000, Invitrogen) and then incubated with 2 U/mL Alexa Fluor 647-conjugated phalloidin (Invitrogen). The F-actin content of cells positive for Iba1 was quantified as the integral intensity of Alexa Fluor 647 fluorescence with a laser scanning cytometer (LSC2, CompuCyte, Cambridge, MA). The mean fluorescent intensity of the cells pretreated with each inhibitor was calculated from the data obtained from 1,000 cells. Increases in membrane ruffles are reported as ratios of the mean fluorescent intensity of the ATP-stimulated cells to that of the unstimulated cells. The effect of the inhibitors was assessed by preincubating cells with wortmannin (Sigma, St. Louis, MO) (100 nM) for 20 min, LY294002 (Wako, Osaka Japan) (50 μM) for 20 min, AR-C69931MX (AstraZeneca, UK) (1 μM) for 10 min, 2′,3′-*O*-(2,4,6-trinitrophenyl) adenosine 5-triphosphate (TNP-ATP) (Invitrogen) (100 μM) for 5 min, pyridoxal-phosphate-6-azophenyl-2′,4′-disulfonic acid (PPADS) (Sigma) (300 μM) for 5 min, or Brilliant blue G (BBG) (Nacalai Tesque, Kyoto, Japan) (1 μM) for 5 min, and then stimulating them with ATP.

Chemotaxis Assay

Dunn chemotaxis chambers (Weber Scientific International, Teddington, UK) were used to perform the chemotaxis assays according to the method described previously (Honda et al., 2001; Webb et al., 1996). In brief, microglia attached to square coverslips were incubated for 4 h in DMEM without FCS. Each coverslip was then inverted onto a chamber and the medium in the outer well was replaced with DMEM containing 50 μM ATP. The chamber was placed on the stage of a microscope (ECLIPSE TE300; Nikon, Tokyo Japan), and cell images were collected every 5 min for 1 h with a CCD camera (Hamamatsu Photonics, Hamamatsu, Japan) and imaging software (fishPPC; Hamamatsu Photonics). Time-lapse video images were used to calculate the final position of cells relative to their starting position, and the distance each cell migrated was measured by plotting the positions of the cell nucleus on a computer display with software (Image-Pro Plus; Media Cybernetics, MD). The distance and direction moved are shown as x and y coordinates on scatter diagrams in which the x-axis is parallel to the outer ring and the position of the outer well is above the y-axis.

Akt Activation

Microglia were incubated for 4 h in DMEM without FCS and then stimulated with 50 μM ATP or 100 ng/mL recombinant murine macrophage-colony stimulating factor (M-CSF) (R&D Systems, Minneapolis, MN) for 5 min at 37°C, and lysed with SDS sample buffer. Proteins were separated by 10% SDS-PAGE and transferred onto an Immobilon P membrane (Millipore, MA). The membrane was incubated for 1 h at room temperature with a blocking solution containing 25 mM Tris, pH 7.5, 150 mM NaCl, 0.1%(v/v) Tween 20 (TTBS), and 5% (v/v) nonfat dry milk, and then incubated overnight at 4°C with mouse monoclonal anti-phospho-Akt (Ser473) antibody (diluted 1:1,000, Cell Signaling Technology, Beverly, MA) or rabbit polyclonal Akt antibody (diluted 1:1,000, Cell Signaling Technology). The membrane was incubated for 1 h at room temperature with horseradish peroxidase (HRP)-conjugated donkey anti-mouse IgG (diluted 1:1,000, GE Healthcare, Little Chalfont, UK) or HRP-conjugated donkey anti-rabbit IgG (diluted 1:1,000, GE Healthcare), and phosphorylated Akt and total Akt were detected with an ECL Western blotting detection system (GE Healthcare). The Akt phosphorylation level was quantified by densitometry with NIH image software. Before stimulating the cells in the calcium-depleted experiment, they were incubated for 30 min in a balanced salt solution composed of 20 mM Hepes, pH7.4, 150 mM NaCl, 5 mM KCl, 1.2 mM $MgCl_2$, and 10 mM glucose in the presence of 1.2 mM Ca^{2+} (BSS) or 1 mM ethy-